THE GEOLOGICAL SOCIETY OF AMERICA®

High-resolution record of multiple organic carbon-isotope excursions in lacustrine deposits of Upper Sinemurian through Pliensbachian (Early Jurassic) from the Sichuan Basin, China

Marco Franceschi[1,2,†], Xin Jin[3], Zhiqiang Shi[3,†], Bin Chen[4], Nereo Preto[5], Guido Roghi[6], Jacopo Dal Corso[7], and Lu Han[3]

[1]*Department of Mathematics and Geosciences, Università degli Studi di Trieste, via Edoardo Weiss, 2, 34128 Trieste, Italy*
[2]*State Key Laboratory of Geological Processes and Mineral Resources, China University of Geosciences (Wuhan), Wuhan 430074, China*
[3]*State Key Laboratory of Oil and Gas Reservoir Geology and Exploitation, Chengdu University of Technology, Chengdu, Sichuan 610059, China*
[4]*School of Geography and Environment, Liaocheng University, Liaocheng 252000, China*
[5]*Department of Geosciences, Università degli Studi di Padova, via Giovanni Gradenigo, 6, 35131 Padova, Italy*
[6]*Institute of Geosciences and Earth Resources–National Research Council of Italy (CNR), via Giovanni Gradenigo, 6, 35131 Padova, Italy*
[7]*State Key Laboratories of Biogeology and Environmental Geology, China University of Geosciences (Wuhan), Wuhan 430074, China*

ABSTRACT

The Sinemurian-Pliensbachian boundary event (ca. 193 Ma) is recorded as a global perturbation of the carbon cycle, as evidenced by a large negative carbon-isotope excursion recorded in many marine sedimentary successions. Whereas multiple lines of evidence testify that the Sinemurian-Pliensbachian boundary event was associated with environmental and climatic changes, sea-level oscillations, and biotic turnovers in marine settings, the record and effects of the event on continents are poorly known. In this paper, we report a high-resolution $\delta^{13}C_{org}$ record and palynological data from the Lower Jurassic lacustrine succession of the Sichuan Basin that allow a prominent 8‰ negative carbon-isotope excursion to be identified at the Sinemurian-Pliensbachian transition. We therefore interpret this perturbation as the expression of the Sinemurian-Pliensbachian boundary event in the Sichuan Basin, and we propose a correlation with the marine realm. Facies evolution illustrates that the Sinemurian-Pliensbachian boundary event coincided with a phase of expansion of the lacustrine systems. Palynological analyses indicate a sharp shift from arid to humid climate conditions coincident with the carbon-isotope perturbation that supports a scenario of lake expansion driven by increased rainfall. In contrast to observations in the Sichuan Basin, where deep lake conditions persisted across the Sinemurian-Pliensbachian boundary event, a global drop in the sea level is documented at the onset of the isotope perturbation. This suggests that eustatic oscillations due to increased continental water storage in lakes and aquifers in the context of a wetter climate phase may have been associated with the early stages of the Sinemurian-Pliensbachian boundary event.

INTRODUCTION

The Sinemurian-Pliensbachian boundary event is recorded as a negative carbon-isotope excursion in both bulk organic matter and carbonate carbon. The Sinemurian-Pliensbachian boundary event was first identified in a Lower Jurassic shallow-marine succession of Yorkshire (UK; Korte and Hesselbo, 2011), and its recognition in carbon from woods and plant fragments indicates a change in the isotopic composition of the ocean-atmosphere-land carbon reservoirs. Multiple examples of evidence of this negative carbon-isotope excursion were later obtained from several marine successions in the Western and Eastern Tethys domains, including series from Italy (Trento Platform and Lombardian Basin; Woodfine et al., 2008; Franceschi et al., 2014, 2019), Morocco (Merino-Tomé et al., 2012; Danisch et al., 2019), France (Paris Basin; Peti et al., 2017), United Kingdom (Korte and Hesselbo, 2011; Ruhl et al., 2016; Storm et al., 2020), and the China (Tethys Himalaya; Han et al., 2021).

According to available biostratigraphic data, the onset of the Sinemurian-Pliensbachian boundary event occurred in the *Echinoceras raricostatum* ammonite Zone, in the late Sinemurian (Korte and Hesselbo, 2011; Storm et al., 2020). By means of astrochronologic calibration, the duration of the Sinemurian-Pliensbachian boundary event has been estimated at ~2 m.y. (Ruhl et al., 2016; Storm et al., 2020).

The magnitude of the Sinemurian-Pliensbachian boundary event (>4‰ in $\delta^{13}C_{org}$) is close to the magnitude of the negative carbon-isotope excursion associated with the early Toarcian ocean anoxic event (e.g., Jenkyns, 1988; Hesselbo et al., 2000, 2007; Suan et al., 2008; Jin et al., 2020), although it stretched over a much longer time interval (2 m.y.), instead of being as abrupt (~300 to ~500 k.y.) as the one in the early Toarcian (Kemp et al., 2005, 2011). There is evidence that in Western Tethys, the Sinemurian-Pliensbachian boundary event coincided with changes in shallow-water carbonate systems. Carbonate platforms changed their depositional geometry and type of carbonate precipitation,

†Corresponding authors: mfranceschi@units.it; marco.franceschi79@gmail.com; szqcdut@163.com.

GSA Bulletin; January/February 2023; v. 135; no. 1/2; p. 3–17; https://doi.org/10.1130/B36235.1; 8 figures; 2 tables; 1 supplemental file.
published online 8 April 2022

which switched from microbial-dominated to skeletal-dominated across the negative carbon-isotope excursion (Wilmsen and Neuweiler, 2008; Franceschi et al., 2019). Recent observations from the Eastern Tethys suggest that these modifications may have had Tethys-wide extent (Han et al., 2021). The Sinemurian-Pliensbachian boundary event is associated with the presence of organic matter preservation intervals and the onset of dysoxic conditions (e.g., Silva et al., 2021). This is supported by sulfur isotope data from Tibet, which are suggestive of organic-rich sediment and pyrite burial (Han et al., 2022). It has been hypothesized that the shift from dysoxic to oxygenated conditions at the end of the Sinemurian-Pliensbachian boundary event triggered the spread of the large, thick-shelled bivalves of the *Lithiotis* fauna on carbonate platforms, at the scale of the entire Tethys Ocean (Franceschi et al., 2014; Han et al., 2021).

The causes of the Sinemurian-Pliensbachian boundary event are still not completely clear. The negative carbon-isotope excursion might be the expression of the injection of isotopically light carbon into the exchangeable reservoirs of the global carbon cycle. In this case, the light carbon could have been derived from the enhanced hydrothermal activity that likely accompanied rifting during the breakup of Pangea (Franceschi et al., 2014). A possible connection with late phases of activity of the Central Atlantic magmatic province has been also hypothesized based on coeval mercury content anomalies reported from the European Southern Alps and United Kingdom (Schöllhorn et al., 2020).

Although the global-scale of the Sinemurian-Pliensbachian boundary event is suggested by its identification in multiple marine successions and by coincident environmental change, the event is poorly known in continental settings (Li et al., 2020). In this paper, we present new high-resolution organic carbon-isotope data from the Sichuan Basin (Southwest China), a large basin that hosted continental sedimentation during a large part of the Mesozoic (SBGM, 1991). We analyzed $\delta^{13}C_{org}$ in the fluvial-lacustrine Ziliujing Formation covering an interval from the Sinemurian to the lowermost Toarcian, which revealed a sharp negative carbon-isotope excursion that, within the constraints provided by the available chronostratigraphy and biostratigraphy, represents the Sinemurian-Pliensbachian boundary event in the Sichuan Basin. Furthermore, we propose a correlation between other features in the $\delta^{13}C_{org}$ record of the Sichuan Basin continental domain and the marine realm and discuss the modifications in the sedimentary environments and sea level across the Sinemurian-Pliensbachian boundary event.

GEOLOGIC SETTING AND STRATIGRAPHY

Marine carbonate sequences dominated the Paleozoic to Middle Triassic Upper Yangtze block, which includes the present-day Sichuan Basin realm. Owing to the late Middle Triassic collision between the Yangtze plate and North China plate (Zhang et al., 1996; Meng and Zhang, 1999; Li et al., 2003), the Sichuan Basin developed as a foreland basin, with an intense erosion of the Middle Triassic succession commonly attributed to tectonic forebulging (e.g., Deng et al., 1982; Li et al., 2003). Above this unconformity, a thick pile of continental sediments was deposited, recording the Mesozoic evolution of tectonics, environment, and climate in Southwest China (Li et al., 2020). The Late Triassic is represented by the Xujiahe Formation (Li and Wang, 2016; Li et al., 2014). Triassic and Lower Jurassic rocks are separated by another unconformity attributed to regional tectonics in most parts of the Sichuan Basin, whereas a conformable boundary is found in its central portion, where deposition appear to have been more continuous (Guo et al., 1996; Li and He, 2014).

The first Jurassic sedimentary unit in the Sichuan Basin is the Ziliujing Formation (Guo et al., 1996; SBGM, 1991). During deposition of the Ziliujing Formation, erosion of the Longmenshan and Micangshan-Dabashan ranges fed clastic material into the basin (Jia et al., 1988; Guo et al., 1996; Liu, 2003). The Sichuan Basin opened toward the Eastern Tethys Ocean to the southwest and was occasionally influenced by marine incursions (Xu et al., 2017).

The Ziliujing Formation overlies the strongly weathered Xujiahe Formation (Upper Triassic) and is composed of variegated and reddish mudrocks (or shales) intercalated with sandstones, siltstones, and bioclastic limestones as well as marlstones (Li et al., 2020), regarded as having been deposited in a large paleolake (e.g., Ma et al., 2009; Li and He, 2014; Wang et al., 2020). The depositional environments included alluvial plain, delta, and shallow and deep lake (Fig. 1). Five units are distinguished in the Ziliujing Formation. They are, in an ascending order, the Qijiang, Zhenzhuchong, Dongyuemiao, Ma'anshan, and Da'anzhai Members (SBGM, 1991; Li et al., 2020). The Qijiang Member has a limited distribution within the southeastern Sichuan Basin.

The Zhenzhuchong Member and Ma'anshan Member mainly consist of variegated and reddish mudrocks, sandstones, and siltstones (SBGM, 1991; Cai, 1988). The Dongyuemiao Member consists of dark-gray and greenish-gray mudrocks or shales interlayered with grayish bioclastic limestones and marlstones rich in bivalve fossils (Meng et al., 2003; Li and Meng, 2003; Wang et al., 2010). The Dongyuemiao Member contains freshwater bivalves such as *Pseudocardinia* (Li and Meng, 2003), and therefore this unit can be attributed to a lacustrine depositional environment (Cai, 1988; Li and Meng, 2003).

The Da'anzhai Member displays facies similar to the Dongyuemiao Member, characterized by dark-gray to black shales and bioclastic limestones (Wang et al., 2010; Li et al., 2020). The ostracod assemblages (Wang et al., 2010) and Re-Os dating (180.3 ± 3.2 Ma; Xu et al., 2017) indicate a Toarcian age for the Da'anzhai Member (Xu et al., 2017).

This study focused on the uppermost portion of the Zhenzhuchong Member and the entire Dongyuemiao and Ma'anshan Members exposed in the Dacao and Liangshuijing sections, located in the northeastern part of Sichuan Basin, where Lower Jurassic successions crop out along a system of anticlines elongated in the NNE-SSW direction (Fig. 1).

METHODS

Log Measurement and Facies Description

The studied sections are located in the Dazhou area and have coordinates of 31°7′59.84″N, 107°21′38.00″E (Dacao) and 31°0′33.33″N, 107°29′14.20″E (Liangshuijing) (Figs. 1 and 2). The two sections were measured, and basic facies description was carried out to construct the stratigraphic logs shown in Figure 3. At Dacao, the section is made of two portions that were correlated in the field by means of marker intervals.

Palynological Analyses

In total, 10 samples were collected within the Dongyuemiao and Ma'anshan Members and processed for palynological analysis. Their stratigraphic positions are shown in Figure 3 and Figure S1[1].

Samples of mudstone and shale weighing ~10 g were disaggregated and treated with 10%

[1]Supplemental Material. Figure S1: Stratigraphic log with the positions of the samples collected for isotope and palynological analyses at the Dacao "A," Dacao "B," and Liangshuijing sections. Table S1: Results of $\delta^{13}C_{org}$ analyses of Dacao "A," Dacao "B," and Liangshuijing sections. Data are expressed in per mil (‰). The stratigraphic height reported (in meters) refers to Figure S1 and therefore to the composite section constructed correlating the two localities. Please visit https://doi.org/10.1130/GSAB.S.19324190 to access the supplemental material, and contact editing@geosociety.org with any questions.

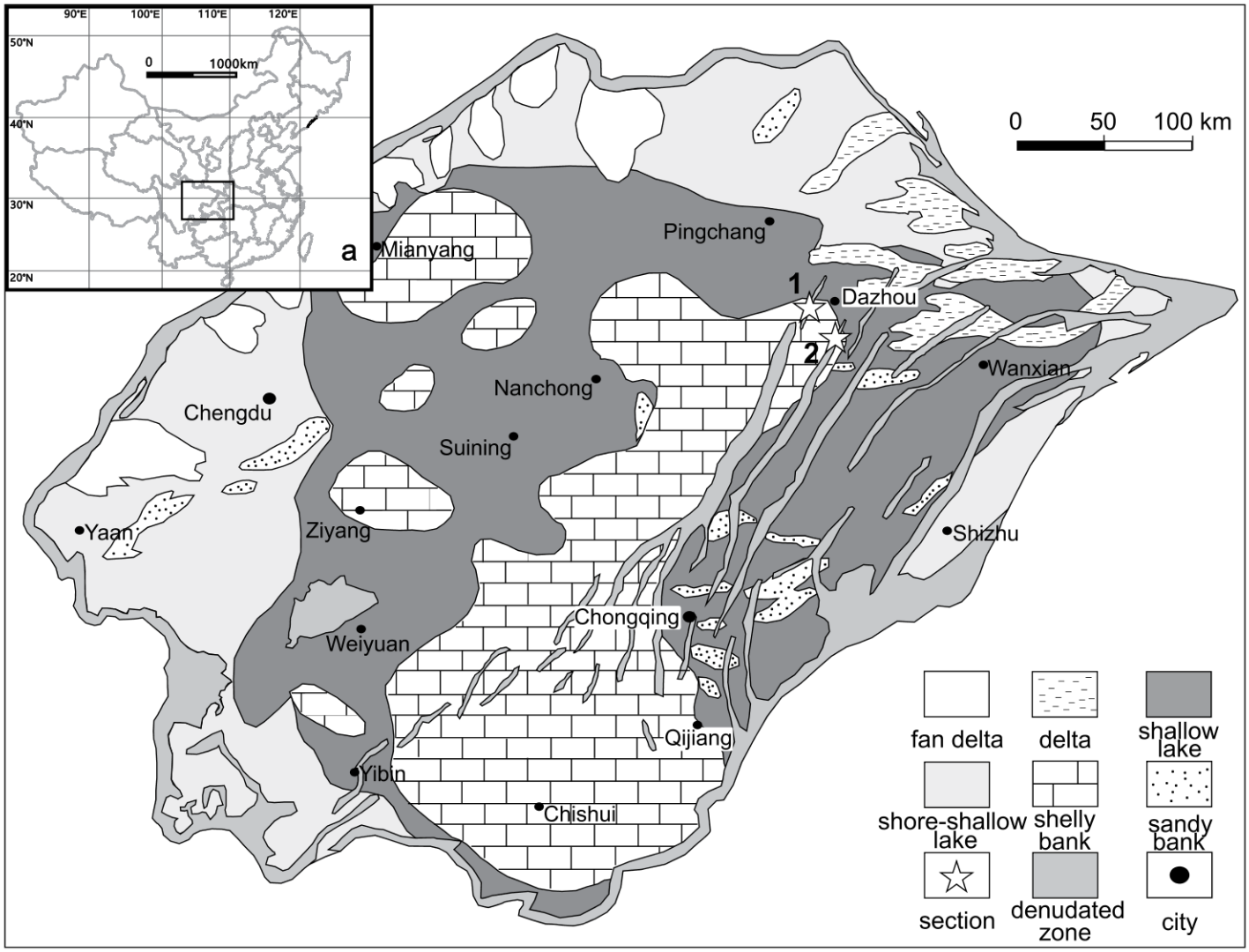

Figure 1. Paleogeographic map of the Sichuan Basin in the Early Jurassic (from EGPG, 1987) showing locations of the Dacao (1) and Liangshuijing (2) sections. Facies mainly refer to the Ziliujing Formation. Coordinates are 31°7′59.84″N, 107°21′38.00″E (Dacao) and 31°0′33.33″N, 107°29′14.20″E (Liangshuijing).

HCl to remove carbonates, followed by dissolution in 47% HF to remove silicate minerals. Residues were washed with deionized water until pH was ~7, and residues were sieved to isolate 10 μm size fractions. Preparations were conducted at the School of Materials and Chemistry and Chemical Engineering, Chengdu University of Technology. Palynomorph-bearing residues were further macerated at the laboratory of the Department of Geosciences at the University of Padova. Upon observation, six samples were productive, which were distributed in the Dongyuemiao and Ma'anshan Members (Fig. 4). The samples were cataloged and stored in the collection of the Institute of Geoscience and Georesources (Consiglio Nazionale delle Ricerche) of Padova.

Sampling and Stable Isotope Analyses

Sampling for $\delta^{13}C_{org}$ analyses was carried out at the Dacao and Liangshuijing sections. Two-hundred and forty-four bulk-rock samples were collected at intervals ranging from 0.2 m to ~1 m from the Ziliujing Formation at Dacao. Sampling covered a total thickness of ~120 m and encompassed the upper part of the Zhenzhuchong Member, the entire Dongyuemiao and Ma'anshan Members, and the lowermost part of the Da'anzhai Member. At Liangshuijing, 85 samples were collected, for a thickness of 35 m, covering the uppermost part of the Ma'anshan Member and the lowermost portion of the Da'anzhai Member (see Fig. S1 in the Supplemental Material for the sampling positions).

Collected samples were mudstone, siltstone, sandstone, and bioclastic limestone. From each sample, ~2 g aliquots of material were inspected for final cleaning, crushed, placed in a polypropylene falcon tube, and treated with a 2 *M* HCl solution for 48 h. The residue was rinsed with deionized water and centrifuged repeatedly until a neutral pH was reached. The sample preparations were conducted at the School of Materials and Chemistry and Chemical Engineering, Chengdu University of Technology. Dried residues were then analyzed for stable isotopes in the mass spectrometry laboratories of the Department of Geosciences at the University of Padova and State Key Laboratory of Ore Deposit Geochemistry, Institute of Geochemistry, Chinese Academy of Sciences, Guiyang.

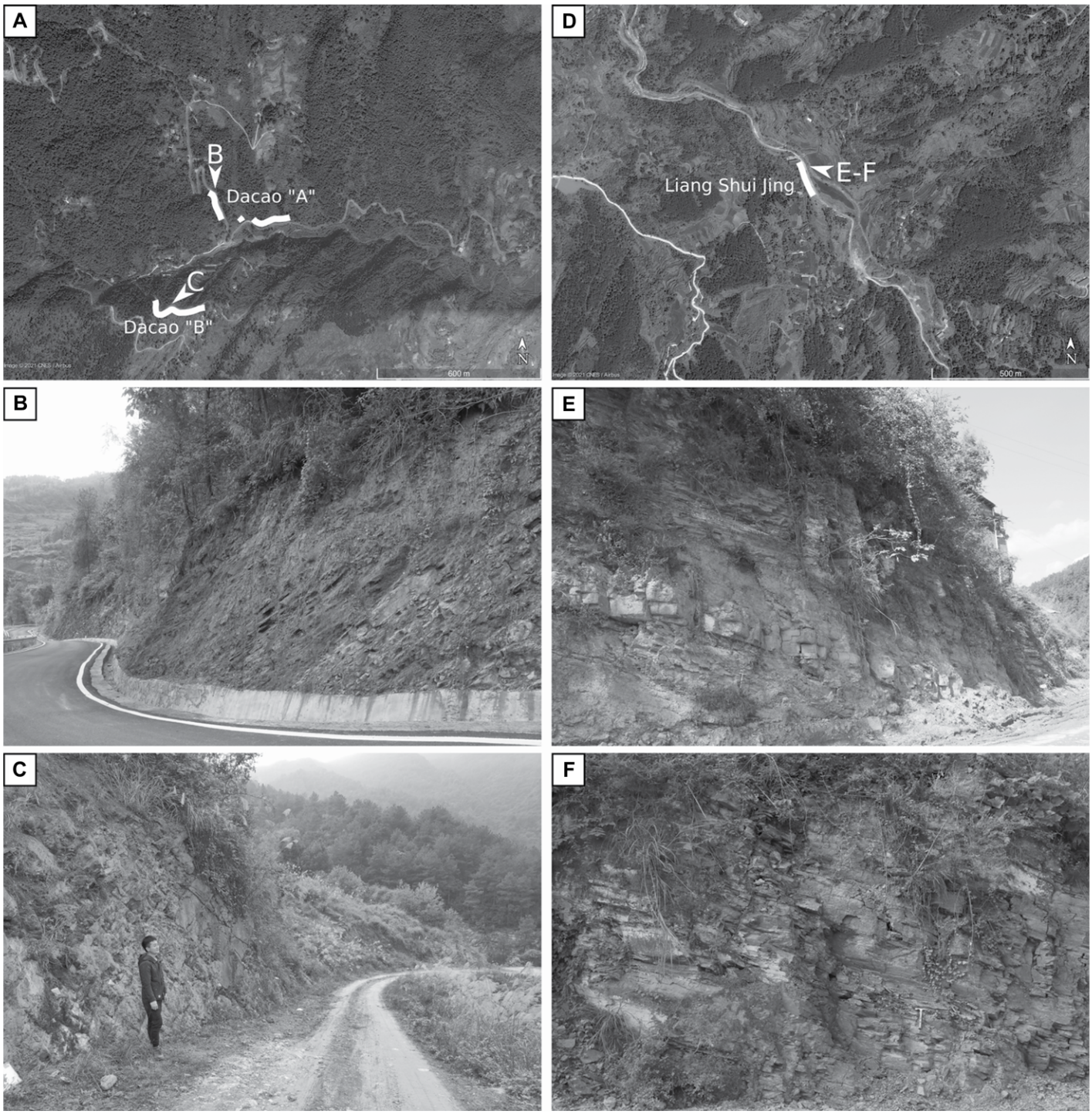

Figure 2. Locations of studied sections and field photographs of the outcrops. (A) Google Earth image showing location of Dacao "A" and Dacao "B" sections (Google Earth, CNES/Airbus Image, date of image 29 September 2019; coordinates 31°7′59.84″N, 107°21′38.00″E). White lines mark the positions of the outcrops. Arrows highlight positions at which photographs displayed in panels B and C were taken. (B) Sandstone facies of the Zhenzhuchong Member at the base of the Dacao "A" section. (C) Sandstone interval at the base of the Ma'anshan Member at Dacao that was used to physically correlate Dacao "A" and Dacao "B." (D) Google Earth image showing location of the Liangshuijing section (Google Earth, CNES/Airbus Image, date of image 8 April 2021; coordinates 31°0′33.33″N, 107°29′14.20″E). White line marks the position of the outcrop. Arrows highlight positions at which photographs displayed in panels E and F were taken. (E) Uppermost portion of the Ma'anshan Member at Liangshuijing. The first shelly limestone layers at the base of the Da'anzhai Member at the Liangshuijing outcrop are in the vicinity of the building visible in the background. (F) Typical appearance of the silty sandstone in the Ma'anshan Member at Liangshuijing.

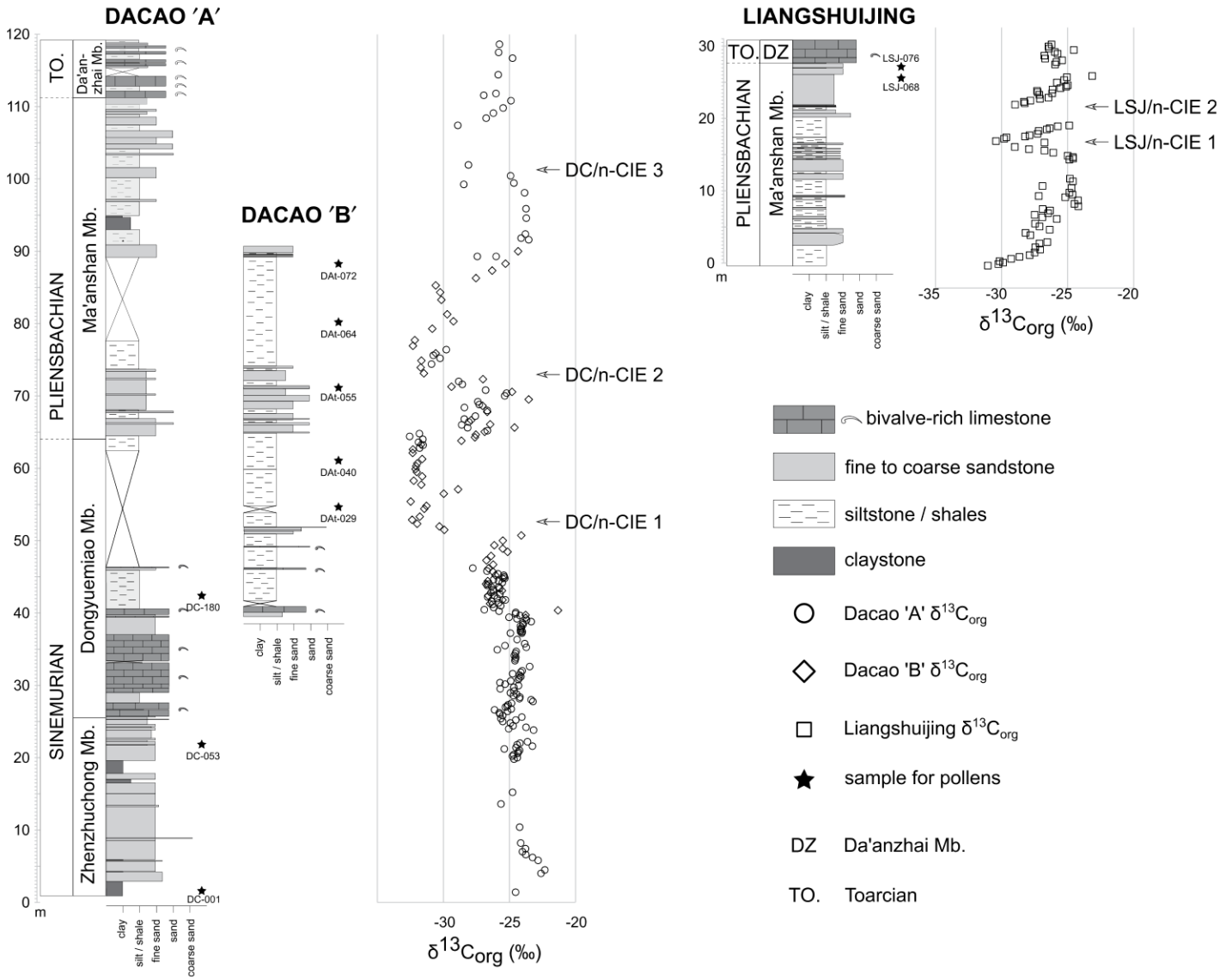

Figure 3. Lithostratigraphic logs and $\delta^{13}C_{org}$ data from Dacao sections (Dacao "A" and Dacao "B") and from Liangshuijing section. Positions of samples collected for palynological investigation are marked by stars. DC—Dacao; LSJ—Liangshuijing; n-CIE—negative carbon isotope excursion.

The mass spectrometer in Padova is a Thermo-Delta VAdvantage linked to a Thermo Flash 2000 Elemental Analyzer. Approximately 0.5–20 mg aliquots of the HCl-etched powder were weighed in tin capsules and fed to the elemental analyzer, where CO_2 for mass spectrometric analysis was developed from the sample via flash burning. Results were calibrated to the international Vienna Peedee Belemnite (VPDB) scale by analyzing contemporaneously two international standards: CH-7 (–32.151‰) and CH-6 (–10.449‰). A quality-control standard was also run along with the samples (ZER sucrose from a C3 plant). The accuracy was ~±0.15‰ (1σ) during the period of the analyses. In Guiyang, a Flash 2000 Elemental Analyzer connected to Finnigan MAT-253 mass spectrometer was used for organic carbon-isotope analysis. One international standard was used, IAEA-C3 (–24.72‰). The analytical precision was better than ±0.1‰.

RESULTS

Lithostratigraphy of Dacao and Liangshuijing Sections

The locations of the Dacao and Liangshuijing sections are shown in Figures 1 and 2, and the stratigraphic logs are shown in Figure 3. The Dacao section encompasses the uppermost portion of the Zhenzhuchong Member, the entire Dongyuemiao and Ma'anshan Members, and the lowermost portion of the Da'anzhai Member. The studied interval is exposed in two outcrops (Dacao A and Dacao B in Fig. 2) that can be easily correlated in the field using marker beds and by facies comparison. In particular, we used a sandstone-rich interval at the base of the Ma'anshan Member to physically correlate the Dacao A and Dacao B outcrops (see Fig. 2C). At Dacao, the Zhenzhuchong Member is mainly composed of fine sandstone with plane-parallel bedding at centimeter to decimeter scale. Some clay layers can also be found. The transition to the Dongyuemiao Member

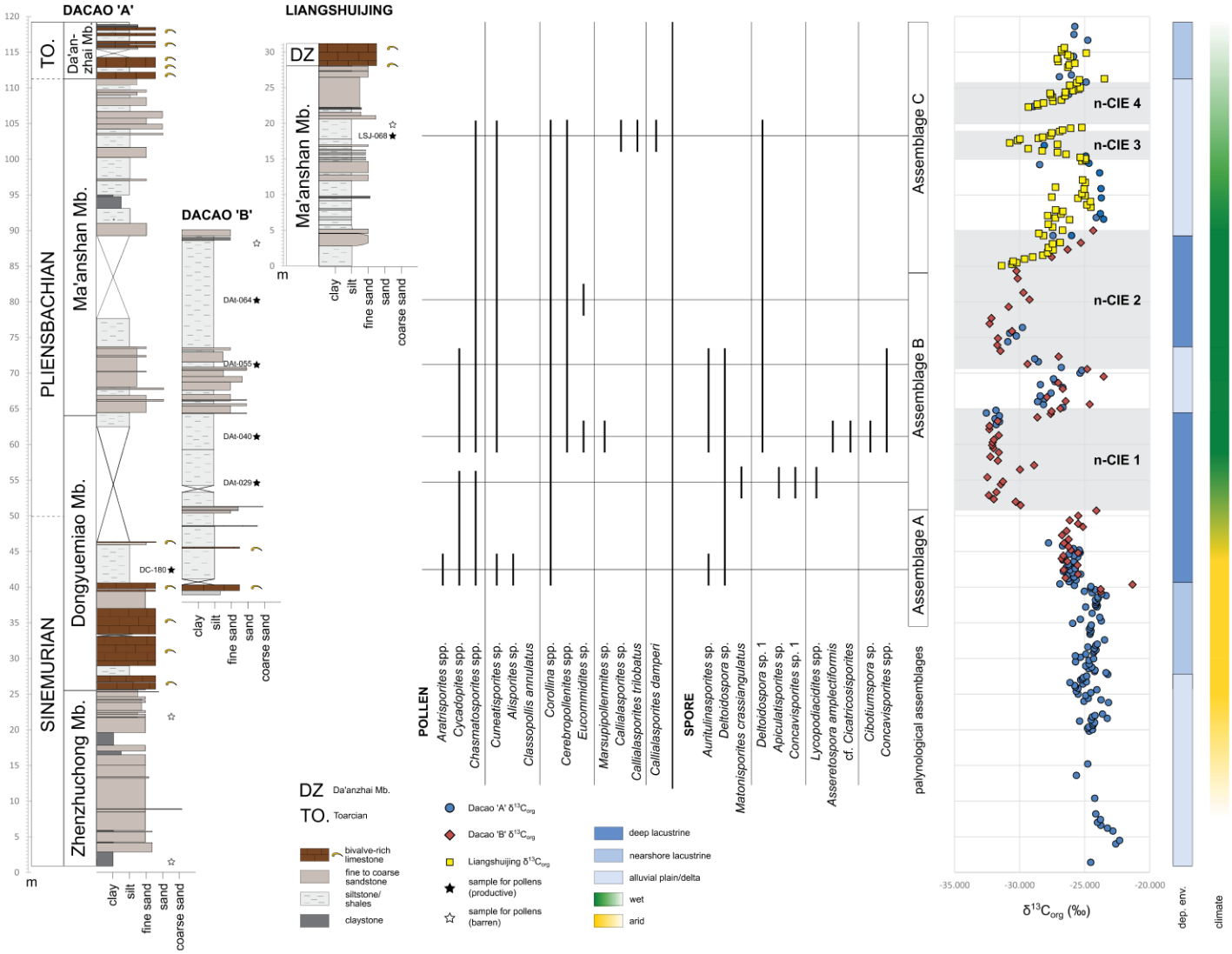

Figure 4. $\delta^{13}C_{org}$ record and palynostratigraphy from the Zhenzhuchong, Dongyuemiao, and Ma'anshan Members of the Ziliujing Formation. The $\delta^{13}C_{org}$ curve derives from the correlation of Dacao (Dacao "A" and "B") and Liangshuijing sections shown in Figure 2. Evolution of the depositional setting of the lacustrine environment and climate conditions is inferred from the identified palynological associations (see also Tables 1 and 2); n-CIE—negative carbon-isotope excursion. See main text for details.

is characterized by the appearance of bivalve-rich beds. Bivalves can be found throughout the Dongyuemiao Member, but in the lower 15 m of the unit, they are particularly abundant. The upper part of the Dongyuemiao Member is dominated by black siltstones and shales that are normally black, dark gray, or dark brown in color, although weathered portions can be yellow or reddish. The total thickness of the Dongyuemiao Member at Dacao was estimated to be ~40 m. The transition to the overlying Ma'anshan Member has been placed where an increase in sandstones occurs at approximately meter level 64 (Fig. 3). The Ma'anshan Member at Dacao comprises mainly gray to dark-gray or black fine sandstone and siltstone with some coarser sand layers. In places, reddish siltstones are found. Bivalve-rich facies that are common in the underlying Dongyuemiao Member are not found in the Ma'anshan Member, although bivalves are still found. The occurrence of vegetal fragments is common throughout the unit. At Dacao, the Ma'anshan Member is ~45 m thick. The contact with the overlying Da'anzhai Member is marked by the occurrence of characteristic bivalve limestone beds associated with black shales.

At Liangshuijing, the upper part of the Ma'anshan Member and the lower part of the Da'anzhai Member are exposed. Only the upper 15 m of the Ma'anshan Member crop out, and they are composed of black, dark-gray, and brown siltstone and gray to dark-gray fine sandstone and sandstone with bivalves and plant fragments. The presence of some yellow clayey layers, reddened surfaces, and levels with carbonate nodules is likely indicative of paleosols/exposure surfaces. The transition to the overlying Da'anzhai Member is marked by the occurrence of the typical bivalve-rich beds above a thin layer of yellow clay on top of a sandstone layer with crusts of iron oxides.

Palynostratigraphy

The qualitative and semiquantitative palynomorph analyses revealed that the studied sections contain three assemblages (A, B, and

TABLE 1. PALYNOLOGICAL ASSEMBLAGES FOUND IN THE ZHENZHUCHONG, DONGYUEMIAO, AND MA'ANSHAN MEMBERS OF THE ZILIUJING FORMATION IN THE DACAO AND LIANGSHUIJING SECTIONS, SICHUAN BASIN, SOUTHWEST CHINA

Assemblage characteristics	Characteristic palynomorphs
Assemblage A Pollen dominated, low diversity; low spore abundance; high cycadean pollen abundance	*Chasmatosporites* spp., *Cycadopites* spp., *Marsupipollenites* sp., *Cuneatisporites* sp., *Alisporites* sp. *Corollina* spp., *Auritulinasporites* sp., *Deltoidospora* sp.
Assemblage B High spore abundance and diversity; decreased pollen diversity and abundance	*Deltoidospora* spp., *Apiculatisporites* spp., *Concavisporites* spp., *Lycopodiacidites* spp., *Asseretospora amplectiformis*, *Auritulinasporites* sp., *Matonisporites crassiangulatus*, cf. *Cicatricosisporites* sp., and *Cibotiumspora* sp. Other pollen taxa are present in low abundances, including *Cycadopites* spp., *Chasmatosporites* spp., *Cuneatisporites* spp., *Cerebropollenites* spp., and *Eucommidites* sp.
Assemblage C Low spore abundance	*Chasmatosporites* spp., *Cuneatisporites* spp., *Corollina* spp., *Cerebropollenites* spp., *Callialasporites* sp. *Deltoidospora* sp.

C in Table 1 and Fig. 4), which are described as follows.

Assemblage A

The pollen taxa characterizing this association were: *Chasmatosporites* spp., *Cycadopites* spp. (Fig. 5J), *Marsupipollenites* sp., *Cuneatisporites* sp. (Fig. 5K), *Alisporites* sp., and different forms belonging to the *Classopollis* groups. The two spore taxa found were *Auritulinasporites* (Fig. 5F) and *Deltoidospora* sp. (Fig. 5A). This association was characteristic of the upper part of the Dongyuemiao Member.

Assemblage B

Spore taxa were dominant in this association: *Deltoidospora* spp., *Apiculatisporites* spp. (Fig. 5E), *Concavisporites* spp. (Fig. 5I), *Lycopodiacidites* spp. (Figs. 5D and 5H), *Asseretospora amplectiformis*, *Auritulinasporites* sp. (Fig. 5F), *Matonisporites crassiangulatus*, cf. *Cicatricosisporites* sp., and *Cibotiumspora* sp. Other pollen taxa were present in low abundances, including *Cycadopites* spp., *Chasmatosporites* spp. (Figs. 6B, 6H, and 6J), *Cuneatisporites* spp., *Cerebropollenites* spp. (Figs. 6A, 6D, 6G, and 6I), and *Eucommidites* sp. This association was characteristic of the uppermost part of the Dongyuemiao Member and lower part of the Ma'anshan Member.

Assemblage C

Pollen taxa became dominant again in this association: *Chasmatosporites* spp. (Figs. 6B, 6H, and 6J), *Cuneatisporites* spp., *Corollina* spp. (Fig. 6E), *Cerebropollenites* spp. (Figs. 6A, 6D, 6G, and 6I), and *Callialasporites* spp. (Figs. 6C and 6F). Spore taxa included *Deltoidospora* sp. This association was found in the upper part of the Ma'anshan Member.

The upper part of the Dongyuemiao Member yielded two different palynofloral assemblages with a clear dominant gymnosperm pollen morphotype (sample DC180, assemblage A) followed by an increase of spore taxa (samples DAt029 and DAt040, assemblage B; Fig. 4).

The lower part of the Ma'anshan Member was always characterized by the abundant presence of spore taxa (assemblage B); in contrast, in the upper part of the Ma'anshan Member, gymnosperm pollen became dominant (assemblage C). Identified spores and taxa are shown in Figures 5 and 6.

$\delta^{13}C_{org}$ Data

The $\delta^{13}C_{org}$ data from the studied sections are displayed in Figure 3. Results of all isotope analyses and positions of the samples are provided as Supplementary Material in Table S1 and Figure S1.

Samples collected at Dacao A and B were plotted together according to the lithostratigraphic correlation made in the field, which is corroborated by the overlap of isotope values and trends (Fig. 3). The $\delta^{13}C_{org}$ values at Dacao ranged from –32.5‰ to –21.3‰. The $\delta^{13}C_{org}$ values were rather constant, around –25‰, in the first 40 m of the section and then underwent first a 1‰ decrease and then remained constant up to meter level 49.5, when an ~2.5‰ negative shift was observed, followed by a 3.8‰ positive excursion. Hence, between meter level 50.5 and 83, $\delta^{13}C_{org}$ values displayed two abrupt negative excursions (DC/n-CIE 1 and n-CIE 2 in Fig. 3, where DC indicates Dacao section). DC/n-CIE 1 encompassed the upper half of the Dongyuemiao Member, between meter level 50.5 and 64, and it had a magnitude of ~8‰. Following a rise of isotope values up to meter level 71 in the lower portion of the Ma'anshan Member, the second negative excursion, DC/n-CIE 2, had a magnitude of ~7‰ and spanned up to meter level 86. Above that, $\delta^{13}C_{org}$ values showed a positive trend that terminated at meter level 91.5. At meter level 101, another fall of ~5‰ in isotope values was recorded (DC/n-CIE3). The uppermost meters of the Ma'anshan Member were characterized by a rise in $\delta^{13}C_{org}$ that reached –25‰ in the first layers of the Da'anzhai Member.

At Liangshuijing section (Fig. 3), which encompassed the upper part of the Ma'anshan Member, isotope data values ranged from –31.3‰ to –23.4‰. The $\delta^{13}C_{org}$ rose ~6‰ from the base of the section up to meter level 9. Then, between meter level 15 and 24, the isotope record was punctuated by two sharp and short negative shifts (LSJ/n-CIE 1 and LSJ/n-CIE 2 in Fig. 3, where LSJ indicates Liangshuijing section) of ~6‰ and 5‰, respectively. After LSJ/n-CIE 2, $\delta^{13}C_{org}$ rose up to around –25‰ at the base of the Da'anzhai Member.

DISCUSSION

Correlation between the Dacao and Liangshuijing Sections

The uppermost portion of the Dacao carbon-isotope curve parallels the $\delta^{13}C_{org}$ record from the Liangshuijing section, both in terms of observed features and isotopic values. The positive trend displayed by $\delta^{13}C_{org}$ in the lower portion of the Liangshuijing section, which culminates with a plateau interrupted by two negative shifts at the top of the Ma'anshan Member (LSJ/n-CIE 1 and LSJ/n-CIE 1 in Fig. 3), is very similar to that seen in the upper half of the Ma'anshan Member at Dacao, where a plateau in $\delta^{13}C_{org}$ is interrupted by DC/n-CIE 3 (Fig. 3). We therefore created a composite $\delta^{13}C_{org}$ curve that combines the data from the Dacao and Liangshuijing sections (Fig. 4). The matching of the features displayed by the $\delta^{13}C_{org}$ record is good, and thicknesses are similar, thus suggesting similar sedimentation rates in the overlapping interval of the two sections. Such a composite curve provides a high-resolution $\delta^{13}C_{org}$ record across the upper part of the Zhenzhuchong Member and the entire Dongyuemiao and Ma'anshan Members. In Figure 4, four major negative carbon-isotope excursions can be identified and are named n-CIE 1, n-CIE 2, n-CIE 3, and n-CIE 4. Figure 7 shows a box plot of the isotope values obtained at Dacao and Liangshuijing versus the main facies where sampling was performed. The box plot highlights that $\delta^{13}C_{org}$ is not facies dependent, although most negative isotope values are found in siltstone.

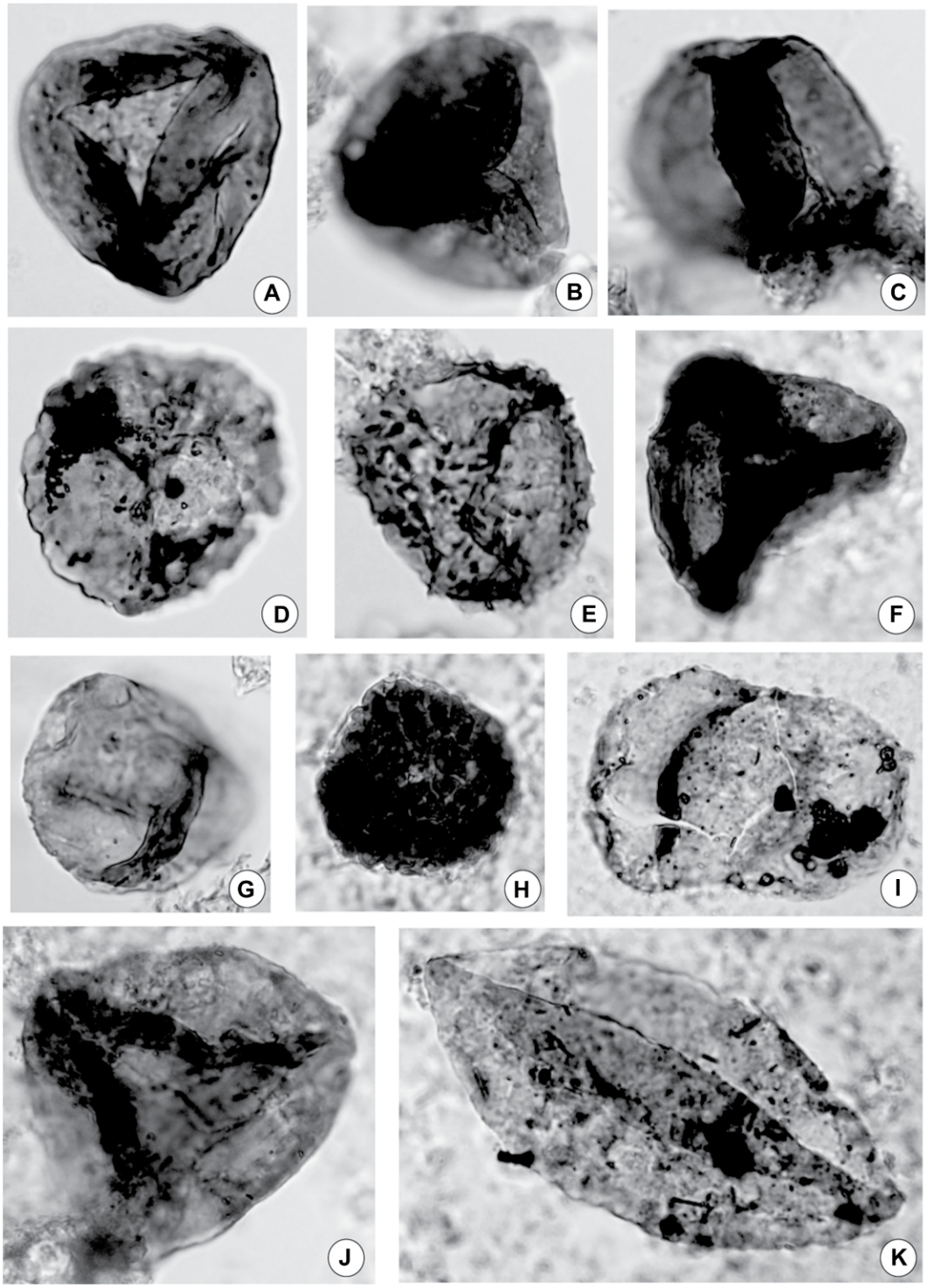

Figure 5. (A) *Deltoidospora* sp., slide DAT029 (VII), S34, diameter 42 µm; (B) trilete spore sp. 1, slide DAT029 (V), N40/1, diameter 40 µm; (C) trilete spore sp. 1, slide DAT029 (VII) P42/2, diameter 40 µm; (D) *Lycopodiacidites* sp., slide DAT029 (VIII) J30, diameter 44 µm; (E) *Apiculatisporites* sp., slide DAT029 (VIII), Q28/4, diameter 36 µm; (F) *Auritulinasporites* sp., slide DAT055 (II), P28/2, diameter 54 µm; (G) trilete spore sp. 1, slide DAT029 (VII), M37, diameter 44 µm; (H) *Lycopodiacidites cerebriformis*, slide DAT64 (IV), O34/3, diameter 40 µm; (I) *Concavisporites* sp., slide DAT055 (II), P45/2, diameter 60 µm; (J) *Cycadopites* sp., slide DC180 (I), P26/4, length 89.6 µm; (K) *Cuneatisporites* sp., slide LSJ068 (II), length 57 µm.

Biostratigraphy and Age

All the productive samples yielded the long-ranging sporomorphs *Cycadopites* spp., *Chasmatosporites* spp., *Cuneatisporites* sp., and different forms of the genus *Classopollis*. These sporomorphs were also reported in the Xujiahe Formation and Zhenzhuchong Member, where the Triassic-Jurassic boundary has been placed (Li-Qin et al., 2020, 2021). The same sporomorphs were found in the assemblage marking the Toarcian oceanic anoxic event in the Fuxian Formation in the Ordos Basin (Jin et al., 2020). The same long-ranging sporomorph specimens could be correlated with the Hettangian-Sinemurian assemblage of South China subprovince described by Liu (2003).

The first appearance of *Callialasporites* spp. in the Ma'anshan Member (sample LSJ068; Fig. 4; Fig. S1) together with the occurrence of the above long-ranging specimens (assemblage C) give useful indications to constrain the age of this unit. *Callialasporites*, a typical genus found

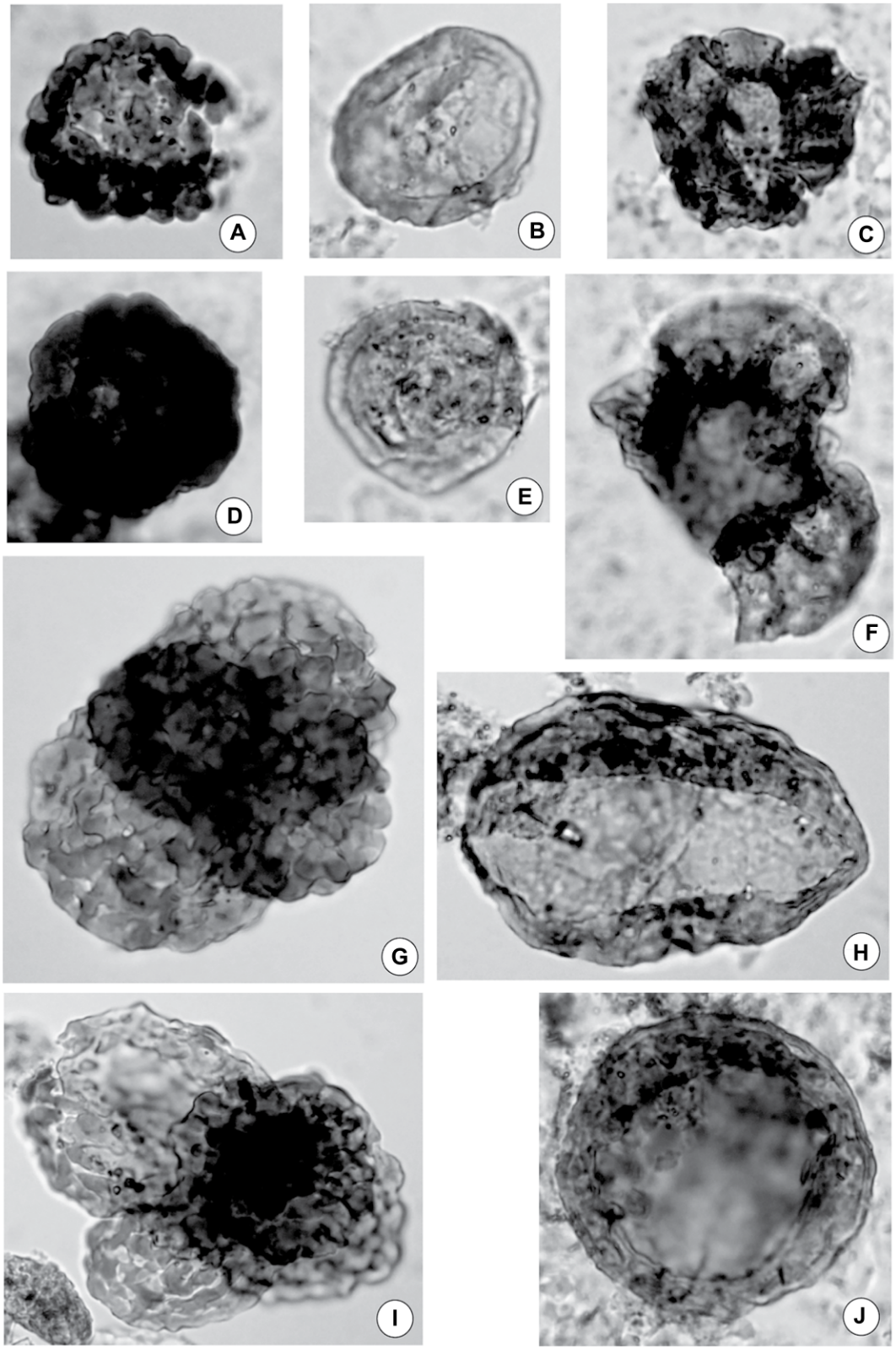

Figure 6. (A) *Cerebropollenites* sp., slide DAT029 (VI), N6, diameter 25 µm; (B) *Chasmatosporites* sp., slide DAT029 (V), Q37/3, diameter 32 µm; (C) *Callialasporites damperi*, slide LSJ068 (III), O37, diameter 30 µm; (D) *Cerebropollenites* sp., slide DAT055 (II), V17/2, diameter 40 µm; (E) *Corollina zwolinska*, slide DAT040 (III), L27/3, diameter 27 µm; (F) *Callialasporites trilobatus*, slide LSJ068 (I), S29/2, diameter 52 µm; (G) *Cerebropollenites* sp., slide DAT029 (VII), M36 K, diameter single grain 45 µm; (H) *Chasmatosporites elegans*, slide DAT029 (VI), Q37/3, length 64 µm; (I) *Cerebropollenites* sp., slide DAT029 (VI), K41, diameter single grain 44 µm; (J) *Chasmatosporites* sp., slide DC180 (I), N33, diameter 49 µm.

in Toarcian sediment in Denmark, Scotland, Spain, Argentina, North Africa, and Kazakhstan (Lund and Pedersen, 1984; Santos et al., 2018, and references therein), had its first appearance in the Pliensbachian of Europe and Greenland (Davies, 1985; Barrón et al., 2013; Koppelhus and Hansen, 2003). *Callialasporites* was found in the Early Jurassic (Pliensbachian–Toarcian) South China palynological subprovince, in the *Dictyophillidites-Cyathidites-Classopollis* assemblage (Liu, 2003), whereas it is absent in the Hettangian–Sinemurian assemblage of the

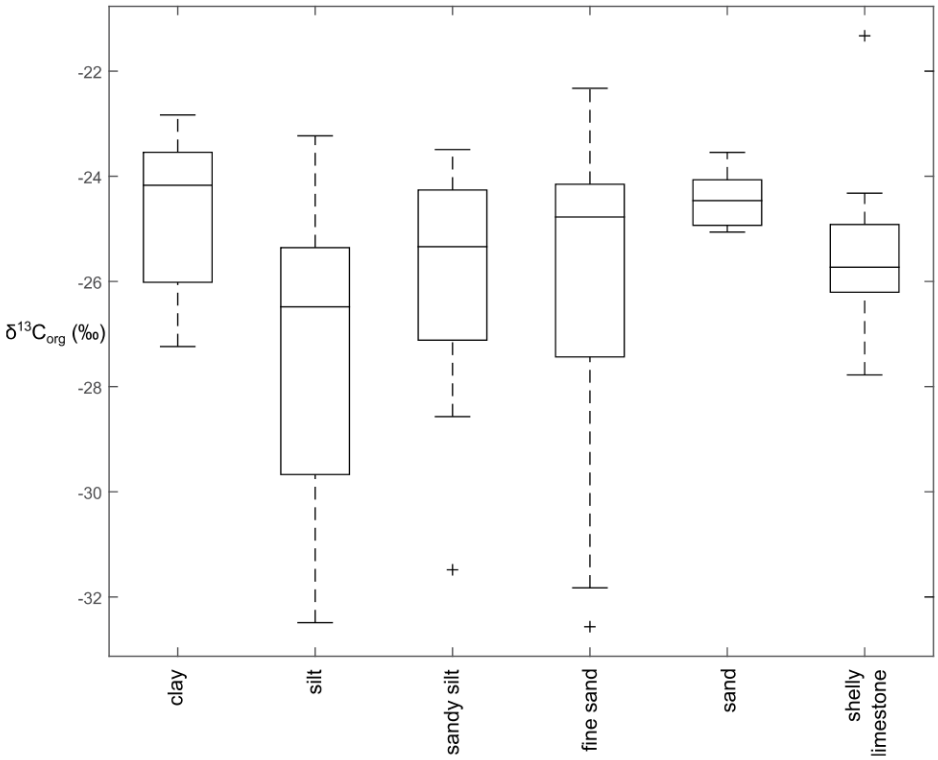

Figure 7. Box plot of main facies at Dacao and Liangshuijing vs. $\delta^{13}C_{org}$. $\delta^{13}C_{org}$ values do not appear to be strongly facies dependent.

South China subprovince. In sum, the identified palynological association fits well within the Lower Jurassic palynological assemblages documented in South China and confirms attribution of the Ma'anshan Member to the Pliensbachian–Toarcian, while the underlying Dongyuemiao and Zhenzhuchong Members can be referred to the Hettangian–Sinemurian.

Additionally, the Ziliujing Formation has been dated to the Early Jurassic on the basis of dinosaur assemblages, aquatic faunas (bivalves, ostracods, conchostracans), floral associations, and palynostratigraphy (Peng, 2009). The Triassic-Jurassic boundary has been positioned close to the boundary between the Zhenzhuchong Member and the underlying Xujiahe Formation, which has been dated to the Norian–Rhaetian based on the rich floras found in the Sichuan Basin (Wang et al., 2010). Re-Os dating carried out on organic matter–rich shales of the Da'anzhai Member has permitted the lowermost portion of this unit to be pinpointed to the Toarcian (Xu et al., 2017). Although uncertainty still exists with regard to the age of the base of the Da'anzhai Member (Liu et al., 2020), available data univocally indicate that the Zhenzhuchong Member, the Dongyuemiao Member, and the Ma'anshan Member represent the Hettangian–Pliensbachian interval. Our palynological data agree with the Lower Jurassic palynological assemblages documented in southern China and therefore confirm this age attribution.

Continental Record of the Sinemurian–Pliensbachian Carbon-Isotope Perturbations and Correlation with the Marine Domain

Our carbon-isotope record from continental successions of the Sichuan Basin shows major negative excursions that can be interpreted in the light of the available biostratigraphic data. Shifts in the isotope ratios could be due to changes in the type of organic matter (e.g., Jin et al., 2019). As stated previously, the Dongyuemiao Member was deposited in a deep lake environment, whereas the Ma'anshan Member comprises fluvial/deltaic facies. As a result, although the presence of terrestrial biomass cannot be excluded, aquatic (algal, bacterial) biomass is likely to be the predominant source of organic matter in the Dongyuemiao Member. Low $\delta^{13}C_{org}$ values (up to –30‰) characterize organic matter from the lacustrine environment (Meyers, 1994). Organic matter from terrestrial plants, on the other hand, usually shows higher $\delta^{13}C_{org}$ values, usually close to –25‰ (Andrusevich et al., 1998). An increase in woody phytoclasts may therefore account for the positive trend in $\delta^{13}C_{org}$ observed in the sandy interval around meter level 70 in the Dacao section (Figs. 3 and 4). As far as thermal diagenesis is concerned, analyses carried out in the upper Da'anzhai Member has evidenced that the organic matter of Early Jurassic successions in the Sichuan Basin may have undergone some thermal alteration (Xu et al., 2021). However, $\delta^{13}C_{org}$ differences in thermally altered organic matter are often small to negligible (Gröcke et al., 2009). Therefore we conclude that, whereas the positive shift at meter level 70 could be due to an increase in the amount of woody material, changes in the source of organic matter and thermal heating do not explain the observed large negative shifts, particularly DC/n CIE-1, which has a magnitude of ~8‰ (Fig. 3) and therefore they can be considered genuine.

The continuous carbon-isotope record provided by Storm et al. (2020) showed that no large isotope excursion is seen in the Hettangian–Sinemurian before the Sinemurian-Pliensbachian boundary event. In agreement with this observation, the isotope record from the Sichuan Basin presented in this study displays a rather flat trend up to meter level 50 in the Dongyuemiao Member, where the first large n-CIE begins (n-CIE 1 in Fig. 4). At Dacao and Liangshuijing, there is no evidence of important erosional surfaces and/or emersions. The coarser lithologies found in the two sections are sandstone layers, whereas the majority of the lithology ranges from silt to fine sandstones. Some reddened surfaces and levels with carbonate nodules are found in the Ma'anshan Member and may indicate possible emersions and the presence of paleosols, but we mainly found them in the Liangshuijing section together with some sedimentary structures such as cross-bedded lamination. Such features are less represented in Dacao, and this may imply that the sedimentary environment in Liangshuijing was shallower and characterized by higher energy. Although the presence of paleosols and evidence of possible subaerial exposure may indicate the existence of some gaps, n-CIE 1 occurs in lacustrine facies (Fig. 4).

From Xu et al. (2017), we know that the base of the Da'anzhai Member is Toarcian; hence, considering the new biostratigraphic constraints and the apparent absence of major stratigraphic hiatuses, we conclude that n-CIE 1 represents the expression of the Sinemurian-Pliensbachian boundary event in the Sichuan Basin. Given that the $\delta^{13}C$ of terrestrial organic matter is strongly controlled by the $\delta^{13}C$ of the atmosphere (Farquhar et al., 1989; Gröcke, 2002; Jahren et al., 2008; Schubert and Jahren, 2013), the identification of the Sinemurian-Pliensbachian boundary event in the terrestrial lacustrine series of the Sichuan Basin strongly supports the fact that this isotope perturbation reflects an important change

in the isotopic composition of the Early Jurassic atmosphere-land-ocean system.

Since the Sinemurian-Pliensbachian boundary event begins in the late Sinemurian *E. raricostatum* ammonite Zone (Korte and Hesselbo, 2011; Storm et al., 2020), its recognition allows us to place the Sinemurian-Pliensbachian boundary within the Dongyuemiao Member (Fig. 4). Overall, our conclusion agrees with results presented by Li et al. (2020), who reported a low-resolution $\delta^{13}C$ curve obtained from pedogenic carbonates and identified a negative carbon isotope excursion at the transition between the Dongyuemiao Member and the Ma'anshan Member, proposing that this shift may well correspond with the Sinemurian-Pliensbachian boundary event. However, in contrast to the observations made by Li et al. (2020), the Sinemurian-Pliensbachian boundary event in the Dacao + Liangshuijing composite $\delta^{13}C_{org}$ curve begins within the Dongyuemiao Member. This discrepancy may be due to diachroneity in the Dongyuemiao Member or to a different definition of the lower and upper boundaries of this unit given in the field, or it could be a result of the higher resolution of our record, which makes it possible to better pinpoint the onset of the carbon-isotope perturbation.

Given the identification of the Sinemurian-Pliensbachian boundary and the Toarcian age of the Da'anzhai Member, it is then possible to correlate the terrestrial composite high-resolution $\delta^{13}C_{org}$ curve of the Sichuan Basin with the coeval records from marine settings.

In Figure 8, we propose a correlation with the Sinemurian-Pliensbachian $\delta^{13}C_{org}$ records from Cardigan Bay Basin of the United Kingdom (Storm et al., 2020) and from the Paris Basin in France (Peti et al., 2017), which represent the most continuous and better age-constrained carbon-isotope records for the Sinemurian–Pliensbachian interval. In doing this, we are aware of two issues. The first is the present lack of other independent chronostratigraphic constraints within the Ziliujing Formation. The second is

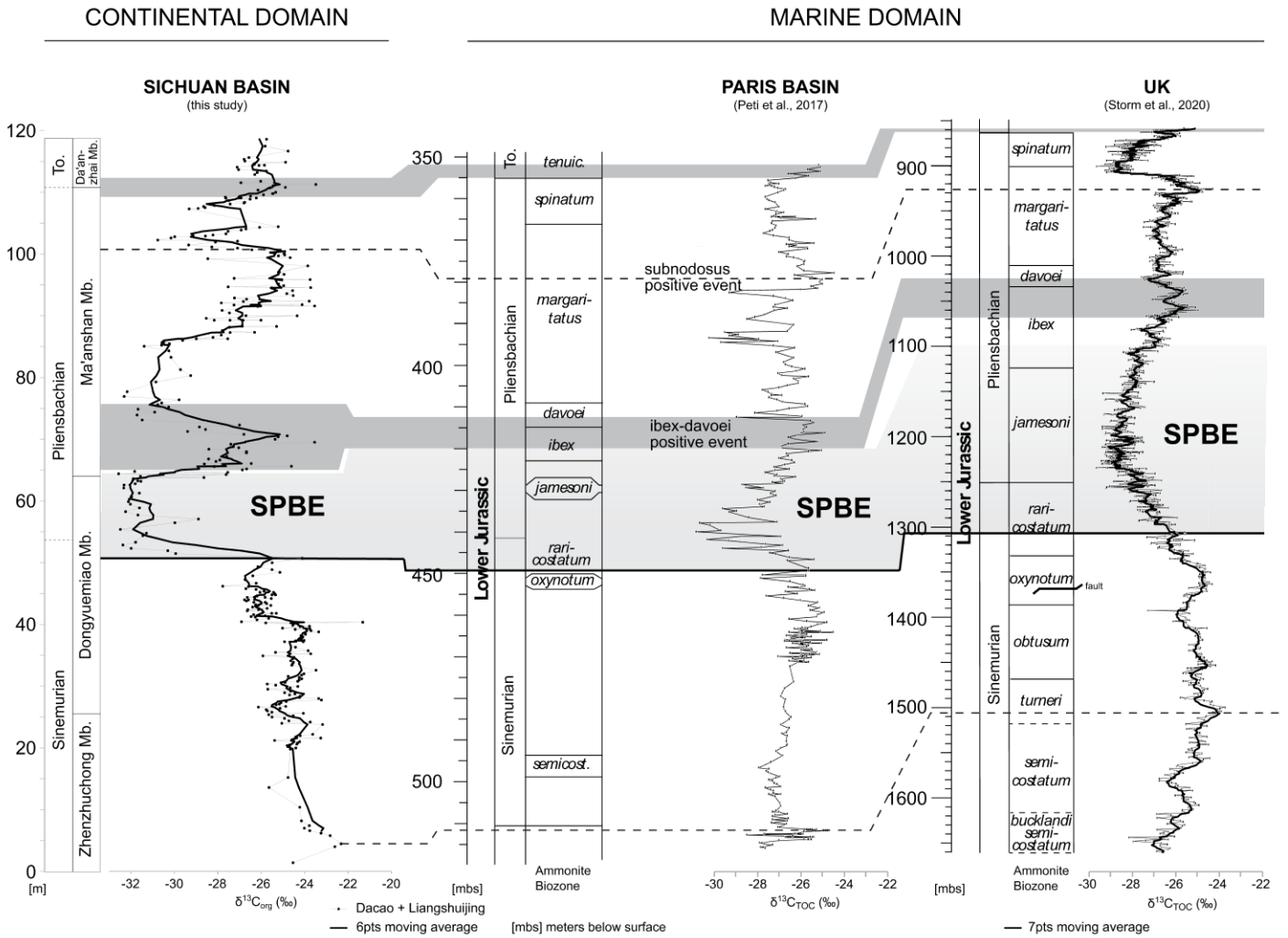

Figure 8. Global-scale correlation of the $\delta^{13}C_{org}$ composite record from the continental Ziliujing Formation (Sichuan Basin, South China) presented in this study with the marine successions of the Paris Basin (Sancerre Couy core; Peti et al., 2017) and United Kingdom (Mochras Borehole; Storm et al., 2020). Light-gray band highlights the Sinemurian-Pliensbachian boundary event (SPBE) negative carbon isotope perturbation. Dashed lines and dark-gray bands mark tentative correlations of other positive and negative shifts in the global $\delta^{13}C_{org}$ record of the Upper Sinemurian–earliest Toarcian. To—Toarcian; TOC—total organic carbon. Ammonite biozones: *bucklandi—Arietites bucklandi*; *semicostatum—Arnioceras semicostatum*; *turneri—Caenisites turneri*; *obtusum—Asteroceras obtusum*; *oxynotum—Oxynoticeras oxynotum*; *raricostatum—Echinoceras raricostatum*; *jamesoni—Uptonia jamesoni*; *ibex—Tragophylloceras ibex*; *davoei—Prodactylioceras davoei*; *margaritatus—Amaltheus margaritatus*; *spinatum—Pleuroceras spinatum*.

the presence of paleosols and potential exposure surfaces in the Ma'anshan Member. This likely implies the presence of some gaps, the extent of which is hard to assess without a high-resolution age model. With these two caveats in mind, we attempted to correlate only the major features of the $\delta^{13}C_{org}$ curve.

In addition to the Sinemurian-Pliensbachian boundary event, the main trends in the marine records of the Paris Basin and United Kingdom (Peti et al., 2017; Storm et al., 2020) and the Sichuan Basin continental record (this study) display significant similarities (Fig. 8). The magnitudes of the $\delta^{13}C_{org}$ negative excursions in the Sinemurian-Pliensbachian boundary event are variable, e.g., ~8‰ in Sichuan Basin, ~6‰ in Paris Basin and ~3‰ in the United Kingdom. This phenomenon could be linked to modulation of the relative abundance of terrestrial and marine organic matter in the different geologic settings.

In the European records, three major broad negative oscillations in the $\delta^{13}C_{org}$ values are separated by two positive maxima, which occur between the Upper Sinemurian (*E. raricostatum* ammonite Zone) and the uppermost Pliensbachian (*Pleuroceras spinatum* ammonite Zone). The Dacao-Liangshuijing $\delta^{13}C_{org}$ composite curve displays a similar pattern between the Dongyuemiao Member (Upper Sinemurian) and the Da'anzhai Member (Toarcian). The n-CIE 1 and n-CIE 2 trends are separated by a positive peak in $\delta^{13}C_{org}$. The n-CIE 2 trend is then separated by another positive excursion from the interval characterized by a broad negative oscillation punctuated by the two sharp n-CIE 3 and n-CIE 4 trends (Figs. 4 and 8).

The positive excursion culminating at meter level 66 at Dacao-Liangshuijing and separating the Sinemurian-Pliensbachian boundary event and n-CIE 2 seems to be correlative to the positive shifts observed around the boundary between the *Tragophylloceras ibex* and *Prodactylioceras davoei* ammonite Zones identified both in the Sancerre-Couy (*ibex-davoei* positive event of Peti et al., 2017) and Mochras cores (Fig. 8). This positive oscillation, presented in both Peti et al. (2017) and Storm et al. (2020), is interpreted as the termination of the Sinemurian-Pliensbachian boundary event. This correlation is proposed as tentative because, as mentioned earlier, the positive excursion of $\delta^{13}C_{org}$ between meter level 63 and 73 coincides with sandier facies, and therefore we cannot exclude the possibility that a contribution in determining the isotope values could be due to increased proportions of woody phytoclasts.

The n-CIE 2 trend and the following rebound of $\delta^{13}C_{org}$ in the Dacao-Liangshuijing section (between meter levels 76 and 101, culminating at meter level 99; Fig. 8) may well correspond with the second broad negative/positive oscillation in the $\delta^{13}C_{org}$ values visible in the marine records from France and United Kingdom between the *P. davoei* and the *Amaltheus margaritatus* ammonite Zones. This oscillation encompasses the "*davoei-stokesi* negative event," the "*stokesi* positive event, the "*subnodosus* negative event," and the "*subnodosus* positive event" of Peti et al. (2017). In the upper *A. margaritatus* ammonite Zone, European records display a sharp decrease in $\delta^{13}C_{org}$ named the "*spinatum* negative event." In the Sichuan Basin record, a sharp negative shift is observed at meter level 101, which initiates an oscillation that is punctuated by two negative spikes and that terminates at the base of the Da'anzhai Member. The position of this negative shift, which is close to the Toarcian Da'anzhai Member, suggests an uppermost Pliensbachian age and therefore makes a tentative correlation to the "*spinatum* negative event" possible (Fig. 8). Finally, the base of the Da'anzhai Member at Dacao-Liangshuijing is characterized by a sharp rise in $\delta^{13}C_{org}$ values. Given the Toarcian age of the Da'anzhai Member, this feature can be correlated to the positive shift observed in both the Paris and Cardigan Bay Basins in the lowermost *Dactylioceras tenuicostatum* ammonite Zone (Fig. 8).

Possible Relations Between Expansion of Lacustrine Systems and Sea Level Across the Sinemurian-Pliensbachian Boundary Event

Although Li et al. (2020) highlighted evidence of phases of semiarid conditions in the Lower Jurassic rocks of the Sichuan Basin, the Dongyuemiao Member and the Da'anzhai Member indicate an expansion and deepening of the lacustrine environments. The Ma'anshan Member (fluvial/deltaic) is overlain by the Da'anzhai Member (lacustrine), indicating a transgressive trend of the lake facies. Furthermore, a deepening trend is observed within the Da'anzhai Member, where the abundant fossiliferous limestones that characterize its lower part, indicating a nearshore environment, are followed by organic-rich black shales indicative of deep lake conditions (Xu et al., 2017). The same evolution is recorded in the Zhenzhuchong Member and the Dongyuemiao Member. The alluvial plain/delta environment of the Zhenzhuchong Member is overlain by the lacustrine Dongyuemiao Member, indicating a transgression of the lacustrine system. In this latter member, again, bioclastic limestone beds are concentrated at the base of the unit and are followed by fine silty facies and gray and black shales indicating a deepening trend (Fig. 4).

The isotope record from Dacao-Liangshuijing reveals that the deposition of the shale facies of the Dongyuemiao Member, i.e., the onset of deeper lake conditions, slightly preceded the Sinemurian-Pliensbachian boundary event (Fig. 4). These elements could suggest that the deepening of the Sichuan Basin lake systems evidenced by the deposition of the Dongyuemiao Member may represent a response to increased runoff. Inferences of pCO_2 by Li et al. (2020) from the Ziliujing Formation showed an increase in the uppermost Zhenzhuchong Member that culminated at values estimated at 3×10^3 ppmV in the Dongyuemiao Member, where the Sinemurian-Pliensbachian boundary event begins. Such evidence seems compatible with an enhancement of hydrological cycling induced by rising atmospheric pCO_2. Furthermore, semiquantitative palynological analyses (Table 2) show an increase of trilete spores and *Cerebropollenites* spp. in the upper part of the Dongyuemiao Member, with a concomitant relative decrease of monolete and bisaccate forms belonging to conifers and *Cycadopites*, while *Circumpolles* are constant with an acme in the lower part of the Ma'anshan Member. This qualitative and quantitative increase of mainly pteridophyte trilete spores, typical of hygrophitic environments, in the uppermost part of the Dongyuemiao Member and lower part of the Ma'anshan Member is indicative of an increase in diversity and a change in climate toward more humid conditions compared to the older terms of the succession (middle/upper part of the Dongyuemiao Member; Fig. 4). In agreement with establishment of wetter climate at

TABLE 2. SEMIQUANTITATIVE ANALYSIS CARRIED OUT ON THE PALYNOLOGICAL ASSOCIATIONS FOUND IN THE DACAO AND LIANGSHUIJING SECTIONS, SICHUAN BASIN, SOUTHWEST CHINA

	DC180	DAT029	DAT064	LSG068
Trilete spore	12	45	20	19
Cycadophytes	55	13	6	4
Conifer (*Cerebropollenites*)	0	15	4	4
Conifer (*Callialasporites*)	0	0	0	15
Bisaccates	12	5	24	27
Circumpolles	21	22	46	31

Note: Trilete spores and *Cerebropollenites* spp. display a clear increase in abundance in the upper part of the Dongyuemiao Member, with a concomitant decrease of monolete and bisaccates forms belonging to conifers and *Cycadophites*. Abundance of *Circumpolles* is rather constant, although an acme occurs in the lower part of the Ma'anshan Member.

the Sinemurian-Pliensbachian boundary event, enhanced continental runoff coincident with the carbon-isotope shift has been documented in marine domains (Western Tethys; Franceschi et al., 2014, 2019; Paris Basin; Bougeault et al., 2017). In sum, multiple lines of evidence suggest that a phase of intensified hydrological cycle, triggered by high atmospheric pCO_2 and global warming, may have occurred at large scale during the Sinemurian-Pliensbachian boundary event and in the continental Sichuan Basin coincided with an expansion and deepening of lacustrine systems.

In the Da'anzhai Member also, Xu et al. (2017) identified a phase of strong expansion and deepening of the Sichuan Basin paleolakes coincident with the early Toarcian ocean anoxic event. They attributed this evolution of the sedimentary environments to an intensification of the monsoonal system triggered by global warming and sea-level rise. This interpretation is supported by the presence of acritarchs in some levels within the middle portion of the Da'anzhai Member, indicating the establishment of a connection between the ocean and the Sichuan lakes during the sea-level highstand that occurred in the *Harpoceras falciferum* ammonite Zone. A similar scenario could be invoked also for the Sinemurian-Pliensbachian boundary event. Indeed, a sea-level highstand occurs in the *Uptonia jamesoni* ammonite Zone where the $\delta^{13}C$ negative perturbation reaches its peak (e.g., Korte and Hesselbo, 2011). A key feature in validating a hypothesis comprising an influence of sea level oscillations on the Sichuan paleo lakes during the Sinemurian–Pliensbachian would be finding evidence of marine insgressions in the facies of the Dongyuemiao Member.

Franceschi et al. (2019) pointed out, however, that the Sinemurian-Pliensbachian boundary event carbon-isotope excursion on the Trento Platform (Southern Alps, Italy) coincided, at least in part, with a subaerial exposure of the carbonate platform top. A sea-level fall followed by a transgression in the *E. raricostatum* ammonite Zone is documented in many Lower Jurassic marine successions across Europe (Haq et al., 1988; de Graciansky et al., 1993; Hesselbo and Jenkyns, 1998; Van Buchen and Knox, 1999; Hesselbo and Coe, 2000; Rosales et al., 2006; Aurell et al., 2003; Gómez and Goy, 2005; Barth et al., 2018), and represents a major sequence boundary (JSi5 cycle boundary of Haq, 2018). Since the Sinemurian-Pliensbachian boundary event begins in the *E. raricostatum* ammonite Zone, Franceschi et al. (2019) hypothesized a possible connection between the climate and environmental changes at the event and this sea-level fall, evoking phenomena such as limnoeustasy or groundwater aquifer eustasy, i.e., short-term sea-level oscillations caused by an increase of continental water storage in lakes, groundwater, and endorheic basins, as a potential cause. In the geologic record, examples of this phenomenon have been described in nonglacial times such as the Cretaceous and Triassic (Wagreich et al., 2014; Sames et al., 2016; Wendler and Wendler, 2016; Wendler et al., 2016; Wang et al., 2022).

Since the Triassic, large lakes formed during the breakup of Pangea, such as in the Newark Basin in the United States (Kent et al., 1995), and others existed in the Early Jurassic (e.g., Junggar Basin, China; Sha et al., 2015). These large basins had the potential to store large amounts of freshwater on continents, and therefore variations in volumes of water contained in them could have influenced sea level. A key element indicative of potential limnoeustasy and/or groundwater aquifer eustasy should be a sea-level fall associated with a contemporaneous rise in the level of lacustrine systems. The evidence of a transgression of lakes in the Sichuan Basin, a sea-level fall, and exposure of the carbonate platform, which can be closely correlated with the onset of the Sinemurian-Pliensbachian boundary event, seems to be consistent with this possibility. Although evidence of climate variability has been reported, and in some cases has been imputed to changes in water depth rather than to global climate changes (Dera et al., 2011; Ullmann et al., 2021), the Early Jurassic is mostly considered a greenhouse time, and the $\delta^{13}C_{org}$ negative peak of the Sinemurian-Pliensbachian boundary event coincides with a time of warming that, following a cold phase in the late Sinemurian, initiated around the Sinemurian-Pliensbachian boundary and culminated in a possible short-lived hyperthermal (Silva and Duarte, 2015). If the identification of the Sinemurian-Pliensbachian boundary event in the Sichuan Basin is correct, then the expansion of lake systems represented by the Dongyuemiao Member was at least in part coincident with this warm period. This seems to further support the limnoeustatic and/or groundwater aquifer eustatic hypothesis, because a contribution from changes in continental ice volume to sea-level oscillations is unlikely. A crucial factor for the verification of this hypothesis will be a high-resolution correlation between the Sinemurian–Pliensbachian marine and continental successions.

In any case, these two scenarios of lake-level variations due to sea-level rise or due to limnoeustasy and/or groundwater aquifer eustasy are not mutually exclusive. It has been indeed shown that the Sinemurian-Pliensbachian boundary event isotope perturbation lasted several million years (at least 4 m.y. according to Ruhl et al., 2016; Storm et al., 2020); therefore, it is possible that a complex, and yet unexplored, interplay among climate change, sea-level oscillations, and lake system expansions and contractions may have occurred during this time of perturbation of global climate.

CONCLUSIONS

A new high-resolution $\delta^{13}C_{org}$ record encompassing the Upper Sinemurian to lowermost Toarcian interval and palynological data were retrieved from the continental (fluvial/lacustrine) succession of the Sichuan Basin (South China). These data allowed the identification of the global Sinemurian-Pliensbachian boundary event and a proposed correlation between key isotopic perturbations in the Sinemurian-Pliensbachian successions of continental and marine realms. Facies changes in the Sichuan Basin indicate that a deepening phase of the lacustrine system occurred during the Sinemurian-Pliensbachian boundary event, suggesting an enhancement of the hydrological cycling that might have been related to the injection of volcanogenic greenhouse gases into the atmosphere that is thought to have been responsible for the carbon-isotope perturbation characteristic of the event. Most notably, while the lacustrine environment of the Sichuan Basin underwent a transgression in the late Sinemurian, a relevant, short-lived sea-level fall occurred, creating subaerial exposure of carbonate platforms in the Western Tethys. This contrasting evolution between sea level and lake level at the onset of the Sinemurian-Pliensbachian boundary event suggests that enhanced freshwater storage in lakes and aquifers may have played a role in determining sea-level oscillations in the Early Jurassic.

ACKNOWLEDGMENTS

We wish to thank Xiaomei Zhou, Qiangwang Wu, He Yin, and Xiaoduan Wang for help in the sample preparation and field work. Yanyan Wang kindly granted usage of the laboratory of the School of Materials and Chemistry and Chemical Engineering at Chengdu University of Technology. The comments of James G. Ogg (Purdue) and Stephen P. Hesselbo (Exeter) greatly helped in improving the quality of this work. This research received funding in the frame of project GPMR201709 of the State Key Laboratory of Geological Processes and Mineral Resources of Wuhan (China). This is a contribution to International Geoscience Programme (IGCP) Project 739 "The Mesozoic–Paleogene hyperthermal events."

REFERENCES CITED

Andrusevich, V.E., Engel, M.H., Zumberge, J.E., and Brothers, L.A., 1998, Secular, episodic changes in stable carbon isotope composition of crude oils: Chemical Geology, v. 152, p. 59–72, https://doi.org/10.1016/S0009-2541(98)00096-5.

Aurell, M., Robles, S., Bádenas, B., Rosales, I., Quesada, S., Meléndez, G., and García-Ramos, J.C., 2003, Transgressive–regressive cycles and Jurassic

palaeogeography of northeast Iberia: Sedimentary Geology, v. 162, no. 3–4, p. 239–271, https://doi.org/10.1016/S0037-0738(03)00154-4.

Barrón, E., Comas-Rengifo, M.J., and Duarte, L.V., 2013, Palynomorph succession of the Upper Pliensbachian–Lower Toarcian of the Peniche section (Portugal): Comunicaçõe Geológicas, v. 100 (Especial I), p. 55–61, https://www.lneg.pt/product/tomo-100-2013/.

Barth, G., Pieńkowski, G., Zimmermann, J., Franz, M., and Kuhlmann, G., 2018, Palaeogeographical evolution of the Lower Jurassic: High-resolution biostratigraphy and sequence stratigraphy in the Central European Basin: Geological Society [London] Special Publication 469, p. 341–369, https://doi.org/10.1144/SP469.8.

Bougeault, C., Pellenard, P., Deconinck, J.F., Hesselbo, S.P., Dommergues, J.L., Bruneau, L., Cocquerez, T., Laffont, R., Huret, E., and Thibault, N., 2017, Climatic and palaeoceanographic changes during the Pliensbachian (Early Jurassic) inferred from clay mineralogy and stable isotope (C-O) geochemistry (NW Europe): Global and Planetary Change, v. 149, p. 139–152, https://doi.org/10.1016/j.gloplacha.2017.01.005.

Cai, S.Y., 1988, Some fresh-water bivalve fossils of the Jurassic Ziliujing Formation from Chongqing and Hechuan, Sichuan [in Chinese with English abstract]: Professional Papers of Stratigraphy and Palaeontology, v. 21, p. 128–154.

Danisch, J., Kabiri, L., Nutz, A., and Bodin, S., 2019, Chemostratigraphy of late Sinemurian–early Pliensbachian shallow-to deep-water deposits of the Central High Atlas Basin: Paleoenvironmental implications: Journal of African Earth Sciences, v. 153, p. 239–249, https://doi.org/10.1016/j.jafrearsci.2019.03.003.

Davies, E.H., 1985, The miospore and dinoflagellate cyst oppel-zonation of the Lias of Portugal: Palynology, v. 9, no. 1, p. 105–132, https://doi.org/10.1080/01916122.1985.9989291.

de Graciansky, P.C., Dardeau, G., Dumont, T., Jacquin, T., Marchand, D., Mouterde, R., and Vail, P.R., 1993, Depositional sequence cycles, transgressive-regressive facies cycles, and extensional tectonics: Example from the southern subalpine Jurassic basin, France: Bulletin de la Société Géologique de France, v. 164, no. 5, p. 709–718.

Deng, K.L., He, L., Qin, D.Y., and He, Z.G., 1982, The earlier Late Triassic sequence and its sedimentary environment in western Sichuan Basin [in Chinese with English abstract]: Oil & Gas Geology, v. 3, no. 3, p. 204–210, https://doi.org/10.11743/ogg19820302.

Dera, G., Brigaud, B., Monna, F., Laffont, R., Pucéat, E., Deconinck, J.-F., Pellenard, P., Joachimski, M.M., and Durlet, C., 2011, Climatic ups and downs in a disturbed Jurassic world: Geology, v. 39, no. 3, p. 215–218, https://doi.org/10.1130/G31579.1.

Editorial Group of Petroleum Geology of China (Sichuan) (EEPG), 1987, Petroleum Geology of China, Volume 10: Sichuan Petroleum Region: Beijing, Petroleum Industry Press, p. 70–72.

Farquhar, G.D., Ehleringer, J.R., and Hubick, K.T., 1989, Carbon isotope discrimination and photosynthesis: Annual Review of Plant Physiology and Plant Molecular Biology, v. 40, no. 1, p. 503–537, https://doi.org/10.1146/annurev.pp.40.060189.002443.

Franceschi, M., Corso, J.D., Cobianchi, M., Roghi, G., Penasa, L., Picotti, V., and Preto, N., 2019, Tethyan carbonate platform transformations during the Early Jurassic (Sinemurian–Pliensbachian, southern Alps): Comparison with the Late Triassic Carnian pluvial episode: Geological Society of America Bulletin, v. 131, no. 7–8, p. 1255–1275, https://doi.org/10.1130/B31765.1.

Franceschi, M., Dal Corso, J., Posenato, R., Roghi, G., Masetti, D., and Jenkyns, H.C., 2014, Early Pliensbachian (Early Jurassic) C-isotope perturbation and the diffusion of the Lithiotis Fauna: Insights from the Western Tethys: Palaeogeography, Palaeoclimatology, Palaeoecology, v. 410, p. 255–263, https://doi.org/10.1016/j.palaeo.2014.05.025.

Gómez, J.J., and Goy, A., 2005, Late Triassic and Early Jurassic palaeogeographic evolution and depositional cycles of the Western Tethys Iberian platform system (eastern Spain): Palaeogeography, Palaeoclimatology, Palaeoecology, v. 222, no. 1–2, p. 77–94, https://doi.org/10.1016/j.palaeo.2005.03.010.

Google Earth Pro, 2021, Google Earth Pro, Version 7.3.4.8248, https://earth.google.com/web (accessed 13 December 2021).

Gröcke, D.R., 2002, The carbon isotope composition of ancient CO_2 based on higher-plant organic matter: Philosophical Transactions of the Royal Society of London A: Mathematical, Physical and Engineering Sciences, v. 360, no. 1793, p. 633–658, https://doi.org/10.1098/rsta.2001.0965.

Gröcke, D.R., Rimmer, S.M., Yoksoulian, L.E., Cairncross, B., Tsikos, H., and van Hunen, J., 2009, No evidence for thermogenic methane release in coal from the Karoo-Ferrar large igneous province: Earth and Planetary Science Letters, v. 277, p. 204–212, https://doi.org/10.1016/j.epsl.2008.10.022.

Guo, Z.W., Deng, K.L., and Han, Y.H., 1996, The Formation and Development of Sichuan Basin [in Chinese]: Beijing, Geological Publishing House, 200 p.

Han, Z., Hu, X., BouDagher-Fadel, M., Jenkyns, H.C., and Franceschi, M., 2021, Early Jurassic carbon-isotope perturbations in a shallow-water succession from the Tethys Himalaya, Southern Hemisphere: Newsletters on Stratigraphy, v. 54, no. 4, p. 461–481, https://doi.org/10.1127/nos/2021/0650.

Han, Z., Hu, X., He, T., Newton, R.J., Jenkyns, H.C., Jamieson, R.A., and Franceschi, M., 2022, Early Jurassic long-term oceanic sulfur-cycle perturbations in the Tibetan Himalaya: Earth and Planetary Science Letters, v. 578, https://doi.org/10.1016/j.epsl.2021.117261.

Haq, B.U., 2018, Jurassic sea-level variations: A reappraisal: GSA Today, v. 28, no. 1, p. 4–10, https://doi.org/10.1130/GSATG359A.1.

Haq, B.U., Hardenbol, J., and Vail, P.L., 1988, Mesozoic and Cenozoic chronostratigraphy and cycles of sea-level change, *in* Wilgus, C.K., Hastings, B.S., Kendall, C.G.St.C., Posamatier, H.W., Ron, C.A., and van Wagner, J.C., eds., Sea-Level Changes—An Integrated Approach: Society of Economic Paleontologists and Mineralogists (SEPM) Special Publication 42, p. 71–108, https://doi.org/10.2110/pec.88.01.0071.

Hesselbo, S.P., and Coe, A.L., 2000, Jurassic sequences of the Hebrides Basin, Isle of Skye, Scotland, *in* Graham, J.R., and Ryan, A., eds., Field Trip Guidebook: International Sedimentologists Association Meeting: Dublin, Ireland, International Sedimentologists Association, p. 41–58.

Hesselbo, S.P., and Jenkyns, H.C., 1998, British Lower Jurassic sequence stratigraphy, *in* de Graciansky, P.C., Hardenbol, J., Jacquin, T., Farley, M., and Vail, P.R., eds., Mesozoic–Cenozoic Sequence Stratigraphy of European Basins: Society for Sedimentary Geology Special Publication 60, p. 561–581, https://doi.org/10.2110/pec.98.02.0561.

Hesselbo, S.P., Gröcke, D.R., Jenkyns, H.C., Bjerrum, C.J., Farrimond, P., Morgans Bell, H.S., and Green, O.R., 2000, Massive dissociation of gas hydrate during a Jurassic oceanic anoxic event: Nature, v. 406, 6794, p. 392–395, https://doi.org/10.1038/35019044.

Hesselbo, S.P., Jenkyns, H.C., Duarte, L.V., and Oliveira, L.C.V., 2007, Carbon-isotope record of the Early Jurassic (Toarcian) oceanic anoxic event from fossil wood and marine carbonate (Lusitanian Basin, Portugal): Earth and Planetary Science Letters, v. 253, no. 3–4, p. 455–470, https://doi.org/10.1016/j.epsl.2006.11.009.

Jahren, A.H., Arens, N.C., and Harbeson, S.A., 2008, Prediction of atmospheric $\delta^{13}CO_2$ using fossil plant tissues: Reviews of Geophysics, v. 46, no. 1, RG1002, https://doi.org/10.1029/2006RG000219.

Jenkyns, H.C., 1988, The early Toarcian (Jurassic) anoxic event: Stratigraphic, sedimentary and geochemical evidence: American Journal of Science, v. 288, no. 2, p. 101–151, https://doi.org/10.2475/ajs.288.2.101.

Jia, C.Z., Shi, Y.S., and Guo, L.Z., 1988, Plate Tectonics of Eastern Qinling Mountains of China [in Chinese]: Nanjing, China, Nanjing University Press, 321 p.

Jin, X., McRoberts, C.A., Shi, Z., Mietto, P., Rigo, M., Roghi, G., Manfrin, S., Franceschi, M., and Preto, N., 2019, The aftermath of the CPE and the Carnian-Norian transition in northwestern Sichuan Basin, South China: Journal of the Geological Society [London], v. 176, no. 1, p. 179–196, https://doi.org/10.1144/jgs2018-104.

Jin, X., Shi, Z., Baranyi, V., Kemp, D.B., Han, Z., Luo, G., Hu, J., He, F., Chen, L., and Preto, N., 2020, The Jenkyns event (early Toarcian OAE) in the Ordos Basin, North China: Global and Planetary Change, v. 193, https://doi.org/10.1016/j.gloplacha.2020.103273.

Kemp, D.B., Coe, A.L., Cohen, A.S., and Schwark, L., 2005, Astronomical pacing of methane release in the Early Jurassic period: Nature, v. 437, p. 396–399, https://doi.org/10.1038/nature04037.

Kemp, D.B., Coe, A.L., Cohen, A.S., and Weedon, G.P., 2011, Astronomical forcing and chronology of the early Toarcian (Early Jurassic) oceanic anoxic event in Yorkshire, UK: Paleoceanography, v. 26, p. PA4210, https://doi.org/10.1029/2011PA002122.

Kent, D.V., Olsen, P.E., and Witte, W.K., 1995, Late Triassic–earliest Jurassic geomagnetic polarity sequence and paleolatitudes from drill cores in the Newark rift basin, eastern North America: Journal of Geophysical Research–Solid Earth, v. 100, no. B8, p. 14,965–14,998, https://doi.org/10.1029/95JB01054.

Koppelhus, E.B., and Hansen, C.F., 2003, Palynostratigraphy and palaeoenvironment of the Middle Jurassic Sortehat formation (Neill Klinter Group), Jameson Land, East Greenland: Geological Survey of Denmark and Greenland (GEUS) Bulletin, v. 1, p. 777–811, https://doi.org/10.34194/geusb.v1.4689.

Korte, C., and Hesselbo, S.P., 2011, Shallow marine carbon and oxygen isotope and elemental records indicate icehouse-greenhouse cycles during the Early Jurassic: Paleoceanography, v. 26, no. 4, PA4219, https://doi.org/10.1029/2011PA002160.

Li, L.Q., and Wang, Y.D., 2016, Late Triassic palynofloras in the Sichuan Basin, South China: Synthesis and perspective: Palaeoworld, v. 25, no. 2, p. 212–238, https://doi.org/10.1016/j.palwor.2015.11.009.

Li, L.Q., Wang, Y.D., Kürschner, W.M., Ruhl, M., and Vajda, V., 2020, Palaeovegetation and palaeoclimate changes across the Triassic-Jurassic transition in the Sichuan Basin, China: Palaeogeography, Palaeoclimatology, Palaeoecology, v. 556, https://doi.org/10.1016/j.palaeo.2020.109891.

Li, L.Q., Wang, Y.D., and Vajda, V., 2021, Palynofacies analysis for interpreting paleoenvironment and hydrocarbon potential of Triassic–Jurassic strata in the Sichuan Basin, China: Palaeoworld, v. 30, no. 1, p. 126–137, https://doi.org/10.1016/j.palwor.2020.04.007.

Li, X.B., and Meng, F.S., 2003, Discovery of fossil plants from the Ziliujing Formation in Hechuan of Chongqing [in Chinese with English abstract]: Geology and Mineral Resources of South China, v. 3, p. 60–65, https://doi.org/10.3969/j.issn.1007-3701.2003.03.011.

Li, Y., Allen, P.A., Densmore, A.L., and Xu, Q., 2003, Geological evolution of the Longmen Shan foreland basin (western Sichuan, China) during the Late Triassic Indosinian orogeny: Basin Research, v. 15, no. 1, p. 117–138, https://doi.org/10.1046/j.1365-2117.2003.00197.x.

Li, Y., Li, H.B., Zhou, R.J., Su, D.C., Yan, L., and Yan, Z.K., 2014, Crustal thickening or isostatic rebound of orogenic wedge deduced from tectonostratigraphic units in Indosinian foreland basin, Longmen Shan, China: Tectonophysics, v. 619–620, p. 1–12, https://doi.org/10.1016/j.tecto.2013.05.031.

Li, Y.Q., and He, D.F., 2014, Evolution of tectonic-depositional environment and prototype basins of the Early Jurassic in Sichuan Basin and adjacent areas [in Chinese with English abstract]: Acta Petrolei Sinica, v. 35, no. 2, p. 219–232, https://doi.org/10.7623/syxb201402002.

Liu, M., Sun, P., Them, T.R., Li, Y., Sun, S., Gao, X., Huang, X., and Tang, Y., 2020, Organic geochemistry of a lacustrine shale across the Toarcian oceanic anoxic event (Early Jurassic) from NE China: Global and Planetary Change, v. 191, https://doi.org/10.1016/j.gloplacha.2020.103214.

Liu, Z.S., 2003, Triassic and Jurassic sporopollen assemblages from the Kuqa depression, Tamir Basin of Xinjiang, NW China [in Chinese with English abstract]: Paleontologia Sinica, v. 190, no. 14, p. 1–244.

Lund, J.J., and Pedersen, K.R., 1984, Palynology of the marine Jurassic formations in the Vardekløft ravine, Jameson Land, East Greenland: Bulletin of the Geological Society of Denmark, v. 33, p. 371–400.

Ma, Y.S., Chen, H.D., Wang, G.L., Xu, X.S., Guo, T.L., and Tian, J.C., 2009, Maps of Tectonic Lithofacies

Palaeogeography in South China (Sinian–Neogene) [in Chinese with English abstract]: Beijing, Science Press.

Meng, F.S., Li, X.B., and Chen, H.M., 2003, Fossil plants from Dongyuemiao Member of the Zhiliujing Formation and Lower-Middle Jurassic boundary in Sichuan Basin, China: Acta Palaeontologica Sinica, v. 42, no. 4, p. 525–536 [in Chinese with English abstract].

Meng, Q.R., and Zhang, G.W., 1999, Timing of collision of the North and South China blocks: Controversy and reconciliation: Geology, v. 27, no. 2, p. 123–126, https://doi.org/10.1130/0091-7613(1999)027<0123:TOCOTN>2.3.CO;2.

Merino-Tomé, Ó., Porta, G.D., Kenter, J.A.M., Verwer, K., Harris, P., Adams, E.W., Playton, T., and Corrochano, D., 2012, Sequence development in an isolated carbonate platform (Lower Jurassic, Djebel Bou Dahar, High Atlas, Morocco): Influence of tectonics, eustacy and carbonate production: Sedimentology, v. 59, no. 1, p. 118–155, https://doi.org/10.1111/j.1365-3091.2011.01232.x.

Meyers, P.A., 1994, Preservation of elemental and isotopic source identification of sedimentary organic matter: Chemical Geology, v. 114, p. 289–302, https://doi.org/10.1016/0009-2541(94)90059-0.

Peng, G.Z., 2009, Assemblage characters of Jurassic dinosaurian fauna in Zigong of Sichuan: The Journal of Geology, v. 33, no. 2, p. 113–123 [in Chinese with English abstract], https://doi.org/10.3969/j.issn.1674-3636.2009.02.113.

Peti, L., Thibault, N., Clémence, M.-E., Korte, C., Dommergues, J.-L., Bougeault, C., Pellenard, P., Jelby, M.E., and Ullmann, C.V., 2017, Sinemurian–Pliensbachian calcareous nannofossil biostratigraphy and organic carbon isotope stratigraphy in the Paris Basin: Calibration to the ammonite biozonation of NW Europe: Palaeogeography, Palaeoclimatology, Palaeoecology, v. 468, p. 142–161, https://doi.org/10.1016/j.palaeo.2016.12.004.

Rosales, I., Quesada, S., and Robles, S., 2006, Geochemical arguments for identifying second-order sea-level changes in hemipelagic carbonate ramp deposits: Terra Nova, v. 18, no. 4, p. 233–240, https://doi.org/10.1111/j.1365-3121.2006.00684.x.

Ruhl, M., Hesselbo, S.P., Hinnov, L., Jenkyns, H.C., Xu, W., Riding, J.B., Storm, M., Minisini, D., Ullmann, C.V., and Leng, M.J., 2016, Astronomical constraints on the duration of the Early Jurassic Pliensbachian Stage and global climatic fluctuations: Earth and Planetary Science Letters, v. 455, p. 149–165, https://doi.org/10.1016/j.epsl.2016.08.038.

Sames, B., Wagreich, M., Wendler, J.E., Haq, B.U., Conrad, C.P., Melinte-Dobrinescu, M.C., Hu, X., Wendler, I., Wolfgring, E., Yilmaz, I.Ö., and Zorina, S.O., 2016, Review: Short-term sea-level changes in a greenhouse world—A view from the Cretaceous: Palaeogeography, Palaeoclimatology, Palaeoecology, v. 441, p. 393–411, https://doi.org/10.1016/j.palaeo.2015.10.045.

Santos, A.A., Wang, X., Fu, Q., and Diez, J.B., 2018, First palynological data from the Jurassic South Xiangshan Formation (Nanjing area, China): Geobios, v. 51, no. 6, p. 559–570, https://doi.org/10.1016/j.geobios.2018.10.002.

Schöllhorn, I., Adatte, T., Charbonnier, G., Mattioli, E., Spangenberg, J.E., and Föllmi, K.B., 2020, Pliensbachian environmental perturbations and their potential link with volcanic activity: Swiss and British geochemical records: Sedimentary Geology, v. 406, https://doi.org/10.1016/j.sedgeo.2020.105665.

Schubert, B.A., and Jahren, A.H., 2013, Reconciliation of marine and terrestrial carbon isotope excursions based on changing atmospheric CO_2 levels: Nature Communications, v. 4, no. 1, p. 1653, https://doi.org/10.1038/ncomms2659.

Sha, J., Olsen, P.E., Pan, Y., Xu, D., Wang, Y., Zhang, X., Yao, X., and Vajda, V., 2015, Triassic–Jurassic climate in continental high-latitude Asia was dominated by obliquity-paced variations (Junggar Basin, Ürümqi, China): Proceedings of the National Academy of Sciences of the United States of America, v. 112, no. 12, p. 3624–3629, https://doi.org/10.1073/pnas.1501137112.

Sichuan Bureau of Geology and Mineral Resources (SBGM), 1991, Geology of Sichuan Province: Beijing, Geological Publishing House, 730 p. [in Chinese with English summary].

Silva, R.L., and Duarte, L.V., 2015, Organic matter production and preservation in the Lusitanian Basin (Portugal) and Pliensbachian climatic hot snaps: Global and Planetary Change, v. 131, p. 24–34, https://doi.org/10.1016/j.gloplacha.2015.05.002.

Silva, R.L., Duarte, L.V., Wach, G.D., Ruhl, M., Sadki, D., Gómez, J.J., Hesselbo, S.P., Xu, W., O'Connor, D., Rodrigues, B., and Mendonça Filho, J.G., 2021, An Early Jurassic (Sinemurian–Toarcian) stratigraphic framework for the occurrence of organic matter preservation intervals (OMPIs): Earth-Science Reviews, v. 221, https://doi.org/10.1016/j.earscirev.2021.103780.

Storm, M.S., Hesselbo, S.P., Jenkyns, H.C., Ruhl, M., Ullmann, C.V., Xu, W., Leng, M.J., Riding, J.B., and Gorbanenko, O., 2020, Orbital pacing and secular evolution of the Early Jurassic carbon cycle: Proceedings of the National Academy of Sciences of the United States of America, v. 117, no. 8, p. 3974–3982, https://doi.org/10.1073/pnas.1912094117.

Suan, G., Mattioli, E., Pittet, B., Mailliot, S., and Lécuyer, C., 2008, Evidence for major environmental perturbation prior to and during the Toarcian (Early Jurassic) oceanic anoxic event from the Lusitanian Basin, Portugal: Paleoceanography, v. 23, no. 1, https://doi.org/10.1029/2007PA001459.

Ullmann, C.V., Szűcs, D., Jiang, M., Hudson, A.J.L., and Hesselbo, S.P., 2021, Geochemistry of macrofossil, bulk rock, and secondary calcite in the Early Jurassic strata of the Llanbedr (Mochras Farm) drill core, Cardigan Bay Basin, Wales, UK: Journal of the Geological Society [London], v. 179, https://doi.org/10.1144/jgs2021-018.

van Buchem, F.S.P., and Knox, R.W.O.B., 1999, Lower and Middle Liassic depositional sequences of Yorkshire (U.K.), *in* de Graciansky P.-C., Hardenbol, J., Jacquin, T., Vail, P.R., eds., Mesozoic and Cenozoic sequence stratigraphy of European Basins: SEPM Special Publication, v. 60, https://doi.org/10.2110/pec.98.02.0545.

Wagreich, M., Lein, R., and Sames, B., 2014, Eustasy, its controlling factors, and the limno-eustatic hypothesis—Concepts inspired by Eduard Suess: Mitteilungen der Österreichischen Geologischen Gesellschaft, v. 107, no. 1, p. 115–131.

Wang, M., Li, M., Kemp, D.B., Boulila, S., and Ogg, J.G., 2022, Sedimentary noise modeling of lake-level change in the Late Triassic Newark Basin of North America: Global and Planetary Change, v. 208, https://doi.org/10.1016/j.gloplacha.2021.103706.

Wang, X., Jin, Z., Zhao, J., Zhu, Y., Hu, Z., Liu, G., Jiang, T., Wang, H., Li, S., and Shi, S., 2020, Depositional environment and organic matter accumulation of Lower Jurassic nonmarine fine-grained deposits in the Yuanba area, Sichuan Basin, SW China: Marine and Petroleum Geology, v. 116, https://doi.org/10.1016/j.marpetgeo.2020.104352.

Wang, Y.D., Fu, B.H., Xie, X.P., Huang, Q.S., Li, K., Li, G., Liu, Z.S., Yu, J.X., Pan, Y.H., Tian, N., and Jiang, Z.K., 2010, The Terrestrial Triassic and Jurassic Systems in the Sichuan Basin, China: Hefei, China, University of Science and Technology of China Press, 216 p. [in Chinese and English].

Wendler, J.E., and Wendler, I., 2016, What drove sea-level fluctuations during the mid-Cretaceous greenhouse climate?: Palaeogeography, Palaeoclimatology, Palaeoecology, v. 441, p. 412–419, https://doi.org/10.1016/j.palaeo.2015.08.029.

Wendler, J.E., Wendler, I., Vogt, C., and Kuss, J., 2016, Link between cyclic eustatic sea-level change and continental weathering: Evidence for aquifer-eustasy in the Cretaceous: Palaeogeography, Palaeoclimatology, Palaeoecology, v. 441, p. 430–437, https://doi.org/10.1016/j.palaeo.2015.08.014.

Wilmsen, M., and Neuweiler, F., 2008, Biosedimentology of the Early Jurassic post-extinction carbonate depositional system, central High Atlas rift basin, Morocco: Sedimentology, v. 55, no. 4, p. 773–807, https://doi.org/10.1111/j.1365-3091.2007.00921.x.

Woodfine, R.G., Jenkyns, H.C., Sarti, M., Baroncini, F., and Violante, C., 2008, The response of two Tethyan carbonate platforms to the early Toarcian (Jurassic) oceanic anoxic event: Environmental change and differential subsidence: Sedimentology, v. 55, no. 4, p. 1011–1028, https://doi.org/10.1111/j.1365-3091.2007.00934.x.

Xu, W., Ruhl, M., Jenkyns, H.C., Hesselbo, S.P., Riding, J.B., Selby, D., Naafs, B.D.A., Weijers, J.W.H., Pancost, R.D., Tegelaar, E.W., and Idiz, E.F., 2017, Carbon sequestration in an expanded lake system during the Toarcian oceanic anoxic event: Nature Geoscience, v. 10, no. 2, p. 129–134, https://doi.org/10.1038/ngeo2871.

Xu, W., Weijers, J.W., Ruhl, M., Idiz, E.F., Jenkyns, H.C., Riding, J.B., Gorbanenko, O., and Hesselbo, S.P., 2021, Molecular and petrographical evidence for lacustrine environmental and biotic change in the palaeo-Sichuan mega-lake (China) during the Toarcian Oceanic Anoxic Event: Geological Society of London, Special Publications, v. 514, p. 335–357, https://doi.org/10.1144/SP514-2021-2.

Zhang, S.G., Wei, C.J., Zhao, Z., and Shen, J., 1996, Formation and metamorphic evolution of the Douling complex from the East Qinling Mountains: Science in China, ser. D, Earth Sciences, v. 39, p. 80–86.

Science Editor: Brad S. Singer
Associate Editor: Daniel Peppe

Manuscript Received 5 July 2021
Revised Manuscript Received 16 December 2021
Manuscript Accepted 8 February 2022

Printed in the USA